Impact Factor 4.9
Q2

Journal of Drug Delivery Science and Technology 111 (2025) 107111

Contents lists available at ScienceDirect

Journal of Drug Delivery Science and Technology

journal homepage: www.elsevier.com/locate/jddst

Folic acid-conjugated Ferulic acid-entangled Single-Walled Carbon Nanotubes: A targeted therapeutic approach for effective breast cancer treatment

Sandra Ross Olakkengil Shajan [a], Shivaraj Kumar Walikar [a], Nandini Markuli Sadashivappa [b], Devaraj Hanumanthappa [b], Basavana Gowda Hosur Dinesh [b], Bandral Sunil Kumar [b], Srinivas Ganjipete [b], Selvaraj Kunjiappan [c], Sankaranarayanan Murugesan [d], Panneerselvam Theivendren [e], Kumarappan Chidambaram [f], Damodar Nayak Ammunje [a,**], Parasuraman Pavadai [b,*]

[a] Department of Pharmacology, Faculty of Pharmacy, M.S. Ramaiah University of Applied Sciences, Bengaluru, 560054, Karnataka, India
[b] Department of Pharmaceutical Chemistry, Faculty of Pharmacy, M.S. Ramaiah University of Applied Sciences, Bengaluru, 560054, Karnataka, India
[c] Department of Biotechnology, Kalasalingam Academy of Research and Education, Krishnankoi, 626126, Tamil Nadu, India
[d] Medicinal Chemistry Research Laboratory, Department of Pharmacy, Birla Institute of Technology and Science, Pilani, Rajasthan, 333031, India
[e] Department of Pharmaceutical Chemistry & Analysis, School of Pharmaceutical Sciences, Vels Institute of Science, Technology & Advanced Studies, Pallavaram, Chennai, Tamil Nadu, 600117, India
[f] Department of Pharmacology, College of Pharmacy, King Khalid University, Abha, 62529, Saudi Arabia

ARTICLE INFO

Keywords:
Breast cancer
Single-walled carbon nanotube
Folic acid
Ferulic acid
DMBA

ABSTRACT

Breast cancer remains one of the major causes of cancer-related deaths in the world for women, which emphasizes the need for better treatment approaches. Conventional therapies target both cancerous as well as normal cells, which can lead to serious adverse effects. This research aimed to develop a targeted therapy employing a new folic acid-conjugated Ferulic Acid-Entangled Single-Walled Carbon Nanotubes (FA-FeA-SWCNTs) formulation to maximize treatment specificity and reduce off-target effects. The efficiency of the FA-FeA-SWCNTs formulation against breast cancer is assessed in this study. Molecular modelling studies were performed to predict the mechanism of action of ferulic acid. FA-FeA-SWCNTs particle size analysis, FTIR, XRD, and SEM were assessed to confirm the formulation tethered to single-walled carbon nanotubes (SWCNTs). MTT assay against MCF-7 cells and CAM assays in chicken eggs were executed to measure cytotoxicity and evaluate anti-angiogenesis efficacy. Sub-acute oral toxicity by OECD 407 guidelines and DMBA-induced breast cancer models in female Wistar rats were used to examine the *in vivo* anticancer efficacy. The potential therapeutic mechanism was suggested by the study's finding that the Ferulic Acid strongly interacted with mitogen-activated protein kinase (MAPK). The formulation showed excellent-, stability, and suitable particle size. Through *in vitro* tests, substantial anti-angiogenic effects (71.2 % inhibition) and significant cytotoxicity (IC_{50} of 19.60 μg/mL) were identified. Subacute toxicity tests verified a favorable safety profile, and *in vivo*, the formulation successfully decreased tumor growth and improved overall wellness, making it a viable option for more clinical investigation.

1. Introduction

The world has been fighting against numerous health crises, and today, new technologies are helping to combat most ailments. However, cancer affects people of all ages and is still one of the world's leading causes of death [1]. Breast cancer continues to be the second most common cancer in women and the leading cause of death for women between the ages of 40 and 59. Breast cancer is still a major global health

* Corresponding author.
** Corresponding author.
E-mail addresses: superdamu@gmail.com, damodar.pg.ph@msruas.ac.in (D.N. Ammunje), pvpram@gmail.com (P. Pavadai).

https://doi.org/10.1016/j.jddst.2025.107111
Received 24 January 2025; Received in revised form 17 April 2025; Accepted 26 May 2025
Available online 2 June 2025

concern even with advancements in early detection, treatment, and screening methods. 5–6 % of breast cancers are inherited, particularly in women with BRCA1 (BReast CAncer gene 1), or BRCA2 (BReast CAncer gene 2), gene mutations [2]. Environmental exposures (ionizing radiation, hazardous chemicals, pollutants) and genetic factors are also contributing factors [3].

Even while targeted therapies and advancements in chemotherapy have raised survival rates, there are still significant clinical gaps [4]. Successfully treating disseminated micro metastases that can contribute to recurrence and overcoming the dose-limiting toxicities of chemotherapy, such as myelosuppression and cardiotoxicity, are two significant challenges to current therapeutic regimens. Despite the development of modified approaches, most current medications only address one of these problems at a time. These limitations highlight the critical need for innovative approaches that can simultaneously target micro metastases and lower systemic toxicity, improving the overall therapy outcome. These challenges can be addressed by the use of nanotechnology and naturally occurring compounds. Phytochemicals have fewer side effects and greater anticancer activity [5]. When these properties, natural compounds can be conjugated with nanotechnologies like single walled carbon nanotubes, this approach can enhance the bioavailability of the drug and reduce adverse reactions. These finding leads to the need to develop such formulation for the effective treatment of breast cancer [6–8].

Based on several reports, one of the potential chemotherapeutic agents is ferulic acid (4-hydroxy-3-methoxycinnamic acid, a hydroxycinnamic acid derived from a polyphenolic compound, shown in Fig. 1 [9]. Ferulic acid (FeA) is found in many plants, particularly in the Ranunculaceae and Gramineae families, which include reed root, *Angelica, Ligusticum chuanxiong, Cimicifuga, Sparganii rhizoma,* etc. Ferulic acid was first extracted and structurally characterized from *Ferula foetida*. FeA is commonly found in grasses, grains, vegetables, flowers, fruits, leaves, beans, coffee seeds, artichokes, peanuts, nuts, and commelinid plants (rice, wheat, oats, and pineapple) [10–16]. Although resveratrol, curcumin, and quercetin are the natural chemicals that show anticancer action, their utilization in drug delivery systems is restricted by factors such as chemical instability, low solubility in water, and poor bioavailability. On the other hand, ferulic acid offers a number of advantages, such as enhanced chemical stability, apoptosis induction and strong antioxidant activity, all of which contribute to its better pharmacological profile [17].

Further, FeA possesses potent free-radical scavenging activity and substantial cytotoxic action and promotes apoptosis in MCF-7 and HepG2 cell lines. It also effectively inhibits cell growth; thus, FeA can be utilized to treat breast cancer efficiently [18]. There isn't any need for extra linker molecules because of its low molecular weight (194 Da) and the presence of carboxyl and hydroxyl groups, which enable direct conjugation with SWCNTs. On the other hand, chemical modifications are frequently necessary for the attachment of larger polyphenols, such as curcumin (368 Da). Because of these characteristics, FeA is more functionally compatible and stable option for targeted drug administration using nanocarriers such as SWCNTs.

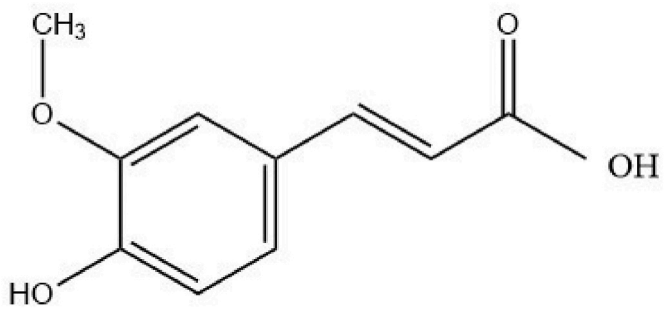

Fig. 1. Structure of Ferulic acid.

Rapidly growing cells require an adequate intake of folate for DNA biosynthesis, repair, and methylation [19]. Folate receptor overexpression observed in breast tumor due to the uptake of more folate for fast proliferation and cell division [20,21]. Folic Acid is a potential ligand for a tumor-targeting agent in drug delivery systems for anticancer therapy because it can bind selectively to the folate receptor (FR), which is overexpressed on tumor cells. When comparing cancerous cells to normal cells, they exhibit 100–300 times higher expression of FR. It is, therefore, a viable option for targeted drug delivery to tumor cells. For this reason, FR is a promising candidate for targeted drug delivery to tumor cells. When folic acid is conjugated to CNTs, it can covalently bind to the folate receptors. As a result, CNTs can easily enter to cell through endocytosis and destroy the cell by releasing the drug [22].

Several nanocarriers, including liposomes, polymeric micelles, quantum dots, carbon nanotubes, and dendrimers, have been utilized to improve the therapeutic effectiveness of anticancer drugs [23]. Due to their unique properties, carbon nanotubes (CNTs) exhibit a specific combination of mechanical, electrical, and optical features and the ability to carry pharmaceutical agents, making them a promising nanomaterial for biomedical applications [23,24]. FA-FeA-SWCNTs offers several advantages compared to other nanocarriers. The conjugated formulation of ferulic acid with SWCNT exhibit enhanced stability and increased potential to effectively treat breast cancer. In contrast, liposomes have poor structural integrity and are rapidly cleared from the body, making them less suitable. This modified formulation also provides more precise targeted drug delivery compared to polymeric nanoparticles. Considering these factors FA-FeA-SWCNTs represents a more effective strategy for the treatment of breast cancer than other nanocarriers system. The objective of the study was to determine the efficacy of Folic acid conjugated Ferulic acid-loaded single-walled carbon nanotube (FA-FeA-SWCNTs) in the treatment of breast cancer in female Wistar rats exposed to DMBA (7,12-dimethylbenz[a]anthracene). DMBA mimics the progression of human breast cancer in rats by causing breast tissue proliferation in the terminal ducts and forming pre-malignant and malignant hyperplastic lesions. The experiments also compared the pure drug (Ferulic acid) and formulation (FA-FeA-SWCNTs) cytotoxicity in MCF-7 cell lines [25].

2. Experimental section

2.1. Chemicals and reagents

Ferulic acid (purity 98 %, formula: $C_{10}H_{10}O_4$), DMSO (Dimethyl Sulfoxide), Doxorubicin Hydrochloride, N-hydroxy succinimide, N-ethyl N' (3-dimethyl- aminopropyl) carbodiimide hydrochloride, and *N-N'*-dicyclohexyl carbodiimide, Triethylamine, and Folic acid procured from SRL. Pvt. Ltd., Bangaluru, and Himedia Laboratories Pvt. Ltd., Mumbai, India. The SWCNTs and DMBA (7,12-dimethylbenz[a]anthracene; molecular weight: 256.3 g $\times$ mol $^{-1}$) were received from Sigma-Aldrich, Bengaluru, India. All other chemicals, reagents, and analytical grade solvents (99 % pure) were used exactly as supplied; no further purification was done.

2.2. Methods

All experiments were conducted according to the guidelines of the National Institutes of Health Guide for the Care and Use of Laboratory Animals and were approved by the Scientific Investigation Board of the institutional animal ethical committee of M. S. Ramaiah University of Applied Sciences as taken to minimize suffering and the number of animals used in the experiments.

3. Materials and methods

3.1. Molecular docking

3.1.1. Protein preparation

The X-ray crystallographic structure of proteins was retrieved from the Protein Data Bank (PDB) (https://www.rcsb.org/) based on the organism, resolution, and other factors using the website https://www.rcsb.org. 23 potent targets were selected against human breast cancer. The identified top 10 proteins showing the best results are KEAP-1 (Kelch-like ECH-associated Protein-1) with (PDB ID: 5GIT), Mitogen-Activated Protein Kinase (MAPK) with (PDB ID: 6E2N), Tubulin Alpha Receptor with (PDB: ID 6S8L), and Human Glyoxalase 1 Receptor with (PDB ID: 7WT0), Abl Kinase with (PDB ID: 2HZI), Renin complex with (PDB ID: 3VUC), VEGF Receptor with (PDB ID 3WZE), Progesterone Receptor with (PDB ID: 3ZR7), Estrogen Receptor with (PDB ID: 5WGD), Epidermal growth factor Receptor with (PDB ID:8A27). The PyMOL program (from Schrödinger, Inc. USA) optimized the protein structure and added hydrogen atoms and missing amino acids to the selected proteins [26].

3.1.2. Ligand preparation

The 3D structure of Ferulic acid (compound id: ID 445858) with the molecular formula $C_{10}H_{10}O_4$ was retrieved from the PubChem database (https://pubchem.ncbi.nlm.nih.gov/) in SDF format, and the ligand was optimized using avagadro tool (https://avogadro.cc/) and further it was used for molecular docking [26].

3.1.3. Molecular docking

Molecular docking was carried out using PyRx tool in Autodock Vina (https://pyrx.sourceforge.io/) to determine the binding potential of Ferulic acid, against twenty-three curated, therapeutically relevant target proteins for breast cancer. The docking analysis results were compared with the reference co-crystal structures. 2D and 3D images of the interactions were generated using the Biovia Discovery Studio Visualizer [27].

3.1.4. ADMET studies

ADMET investigations assess the drug's potential toxicity and how the body metabolizes, distributes, absorbs, and excretes it. This was performed using an online tool called pkCSM using the website https://biosig.lab.uq.edu.au/pkcsm/ [28].

3.1.5. Molecular dynamics simulation

Binding stability, confirmation and interaction modes of the Ferulic acid, KEAP-1, MAPK, Tubulin Alpha receptor, and Human Glyoxalase 1 receptor were analyzed by the molecular dynamic's simulation of 100 ns, 200 ns and 1000 ns, respectively. The DESMOND v3.6 program performed molecular dynamics simulation on the ligand-receptor complex [29]. An orthorhombic periodic boundary was created using pre-set TIP3 water model at a distance of 10-Å units. The addition of the required counterions neutralizes the electric charges. Through equilibrium and heating, the system lowered its energies before the start of the molecular dynamic simulation. The system production step lasted 100 ns, 200 ns, and 1000 ns with time steps of 12 ps; the Nose-Hoover technique and the NPT (isothermal-isobaric) ensemble were utilized, along with 300 K temperature and 1 atmospheric pressure. The complex's interactions and dynamic properties were considered while selecting the best confirmations [30].

3.2. Formulation of FA-FeA-SWCNTs

3.2.1. Synthesis of FA-NHS

The FA-NHS was synthesized as per our previous procedure with minor modifications. In a reaction vessel, folic acid (FA) (3.40×10^{-3} mol) was mixed in anhydrous DMSO (25 mL). N-hydroxysuccinimide (3.87×10^{-3} mol), *N, N′*-dicyclohexylcarbodiimide (5.09×10^{-3} mol), and triethylamine (2.5×10^{-3} mol) were added. The mixture was continuously stirred at 40 °C in a thermostatic water bath for 48 h at 80 rpm in the dark to form FA-NHS [31]. The 0.45 μm filtration eliminated the precipitated DCU (1,3-Dicyclohexylurea). Deionized water (12–24 h, 4–5 exchanges) was dialyzed against the crude product (5–6 kDa MWCO) in order to remove unreacted FA, DMSO and small molecules byproducts. After being purified, the FA-NHS solution was lyophilized to produce a stable form that was kept out of direct sunlight. FTIR (Shimadzu IR Tracer-100, resolution: 4 cm^{-1}, wavelength range: 4000–400 cm^{-1}) was used to characterize the synthetic FA-NHS.

3.2.2. Conjugation of FA-NHS with SWCNTs

Carboxylated-SWCNTs (20 mg) were dispersed in the mixture of 0.261×10^{-3} mol of N-ethyl-N′-(3 dimethyl-aminopropyl) carbodiimide hydrochloride (EDAC) in 20 mL anhydrous DMSO in the reaction bottle with continuous stirring (100 rpm) at 50 °C for 10 h. The solution of FA-NHS (4.60 mg/mL) was added to it with constant magnetic stirring at 100 rpm for 5 days. After the reaction the remaining product was purified by dialysis membrane (5–6 kDa MWCO, HI Media, Mumbai, India), versus deionized water to wash way the un-conjugated FA-NHS. The obtained nanoconjugate was vacuum dried, the pure product was collected and examined using ATR-FTIR spectroscopy [32].

3.2.3. Ferulic acid loading into FA-SWCNTs

By the use of probe sonication (100 W, 5 min pulse mode), a 5 mL suspension of FA-SWCNTs (5.10 mg/mL) was dispersed in a phosphate buffer solution (25 mL, pH 6.1). 25.8×10^{-6} mol of Ferulic acid dissolved in 20 mL of ethanol was added dropwise to the mixture while being continuously stirred by magnetic stirring at 200 rpm at 25 °C in the dark. The ethanol was then extracted from the mixture using a rotary evaporator set at 40 °C and a low pressure. The following suspension was centrifuged at 25,000 rpm, 15 min, and 25 °C. The resultant suspension was repeatedly rinsed with deionized water until supernatant turned transparent, implying that all of the unbound Folic Acid had been removed. The FeA loaded FA-SWCNT were stored in an amber colored container within a desiccator for later use [31,33].

3.2.4. Characterization studies of FA-FeA-SWCNTs

FTIR spectroscopic analysis of ferulic acid, FA-NHS and FA-FeA-SWCNTs were conducted to identify the interaction between drug and FA-FeA-SWCNTs formulation using Bruker Alpha II; the samples were placed on the surface and IR transmittance data over the wave number range of about 3500-820 cm $^{-1}$ measured. Next, the particle size of the FA-FeA-SWCNTs formulation was performed using a Particle size analyzer on a Malvern NanoZS, Malvern Instruments Ltd., in Worcestershire, United Kingdom. Deionized water was used to dilute the samples in a 1:20 ratio, and the readings were taken at 25 °C and a 90°-scattering light. Dynamic scattering light was used to calculate the z average based on the intensity of scattered light. The surface charge of the FA-FeA-SWCNTs particles was measured by zeta potential with the instrument Zetasizer Ver. 6.32 (Malvern Instruments Ltd, Worcestershire, United Kingdom) to check the stability of the suspension, higher zeta potential indicates better stability [34]. The physical characteristics of the FA-FeA-SWCNTs were evaluated by X-ray diffraction with a BRUKER D8 Advance ECO XRD system equipped with an SSD160 1D Detector. The XRD was operated at a voltage of 20 keV and a current of 30 mA using Cu Kα 1 radiation ($\lambda = 1.540\ 60$ Å) in a θ-2θ configuration. The 2θ scan range was set from 5° to 60° with a step size of 0.02° and a scan speed of 2 s per step. SEM analysis was performed using a chamber of model JEOL JSM-6390LV; accelerating voltage is set to 15 kV, and SEM will generate high-resolution images for detailed analysis of the size, shape, and structure of freshly prepared FA-FeA-SWCNTs [35].

3.2.5. Evaluation of ferulic acid encapsulation efficiency and loading capacity

Ferulic acid loading capacity (LC%) and encapsulation efficiency (EE %) into FA-SWCNTs were measured using the previously described methods. The freshly formulated FA-FeA-SWCNTs were centrifuged at 10000 rpm for 15 min. The concentration of Ferulic acid in the supernatant was measured using a UV–visible spectrophotometer, and the absorbance of Ferulic acid was measured at 320 nm [36]. The encapsulation efficiency and drug loading capacity were evaluated by the absorbance values obtained from the calibrated standard plots. The absorbance values were then converted into the amount of Ferulic Acid using the following equations: Eq. (1) and Eq. (2).

$$EE\% = \left(\frac{FeA_{\ loaded}}{FeA_{\ initial}}\right) \times 100 \quad \text{Eq.1}$$

Where.

$FeA_{\ loaded}$ = Amount of FeA loaded from FA-FeA-SWCNTs
$FeA_{\ initial}$ = The initial amount of FeA utilized to prepare FA-FeA-SWCNTs

$$LC\% = \left(\frac{FeA_{\ incorporated}}{FA - FeA - SWCNT_{total}}\right) \times 100 \quad \text{Eq.2}$$

Where.

$FeA_{incorporated}$ = Amount of FeA incorporated in FA- FeA- SWCNT
$FA - FeA - SWCNT_{total}$ = Total amount of FA-FeA-SWCNT formulation

To calculate the LC% of folic acid onto SWCNTs, the quantity of FA bound to SWCNTs was first determined. This was achieved by subtracting the quantity of free FA remaining in the supernatant from the total amount of FA that was initially added. The total weight of the FA-SWCNT conjugate was determined after lyophilization [37]. The following equation was then used to determine the LC% of Folic Acid:

$$LC\% = \left(\frac{FA\ bound\ to\ SWCNT}{Total\ weight\ of\ FA - SWCNT}\right) \times 100 \quad \text{Eq. 3}$$

3.2.6. In vitro drug release study

The release of Ferulic acid from FA-FeA-SWCNTs was detected using a dynamic membrane filtration approach in two different buffers: 0.01 M Acetate buffer (pH 3.4) and 0.01 M Phosphate buffer (pH 7.3) at 37 ± 1 °C. 50 mg of precisely weighed FA-FeA-SWCNTs were shaken in a rotary shaker at 100 rpm at 37 ± 1 °C. The membrane filtration bag with a 3500 Da molecular weight was placed within a beaker containing 30 mL of buffer solutions. The particles were then separated using centrifugation. To maintain a uniform release medium volume, the samples taken out were replaced with new samples at predetermined intervals. UV–visible spectrometry was employed to measure the quantity of drug (Ferulic Acid) released from FA-FeA-SWCNTs at 320 nm, following the collected supernatant was mixed with ethanol [32]. This experiment was conducted for 42 h. The calculation was done with Eq. 4

$$\text{Drug release rate } (\%) = (A_0 - A_1) \times 100 \,/\, A_0 \quad \text{Eq. 4}$$

Where A_0 represents the absorbance of the control, and A_1 represents the absorbance of the sample.

3.3. Evaluation of the cytotoxicity of FA-FeA-SWCNTs

3.3.1. MTT assay

The cytotoxic potential of FA-FeA-SWCNTs was assessed against breast cancer cells (MCF-7 Cell lines). 1×10^5 growing MCF-7 cells were seeded per well in a 96-well culture plate and incubated for 24 h at 37 °C. After 24h of cell growth, cells were incubated with various concentrations of (100, 50, 25, 12.5, 6.25, 3.125 μg/mL) FA-FeA-SWCNTs, and 0.25 μM Doxorubicin for another 24h. Following two phosphate-buffered saline (PBS) washes, the wells were filled with 20 μL of the MTT staining solution, and the plate was incubated at 37 °C for 4 h [38]. Following a 4 h period, 100 μL of DMSO was added into every well to dissolve the formazan crystals, and the absorbance was measured using a microplate reader at 570 nm Cell viability was calculated by the formula:

$$\text{Surviving cells } (\%) = \frac{Mean\ \ OD\ of\ the\ test\ compound}{Mean\ OD\ of\ Negative\ control} \times 100$$

3.3.2. Apoptosis assay

The induction of apoptosis by FA-FeA-SWCNTs was investigated using dual fluorescence labelling with Acridine Orange (AO) and Ethidium Bromide (EB). MCF-7 cells cultured in a 24-well plate were administered the IC_{50} concentration of FA-FeA-SWCNTs and incubated for 48 h [39]. Following two washes of the cells with PBS, 1 μL of the AO/EB dual fluorescent staining solution (each at a concentration of 100 μg/mL, soluble in PBS) was added and incubated for 30 min. Following incubation, the cells were harvested using trypsinization and washed three times with ice-cold PBS. Ten microliters of dyed cells were deposited onto a transparent microscope slide, covered with a coverslip, and examined for apoptotic cell morphology at a magnification of 20× utilizing a Nikon OPTIPHOT-2 fluorescence microscope [40].

3.4. In ovo assay

The candling procedure evaluated the egg's fertility and viability studies. Following this first evaluation, the eggs were incubated for two days at 37 °C. In order to identify blood vessels, another candling process was used, and the eggs were appropriately marked. On the wide side of every egg, a 1 cm^2 window was meticulously made to assess the degree of embryonic blood vessel development. After that, the FA-FeA-SWCNTs formulation was incorporated. High dose group (n = 3) received 12 μg/mL of FA-FeA-SWCNTs, the mid-dose group (n = 3) received 6 μg/mL of FA-FeA-SWCNTs and a low-dose group (n = 3) received 3 μg/mL of FA-FeA-SWCNTs, control group (n = 3) received normal saline. In contrast, the standard group (n = 3) received 0.1 mL of Doxorubicin. After the windows were covered with parafilm, the eggs were re-incubated for three more days. Following the incubation duration, the branching patterns and points of the blood vessels were examined to determine the impact of the formulations provided [41]. The % inhibition was calculated using the formula below:

$$\%\ \text{Inhibition} = \frac{Control - test}{Control} \times 100$$

3.5. Sub-acute toxicity studies

The sub-acute toxicity of the FA-FeA-SWCNTs formulation was evaluated on the test animals over a period of 28 days. During that time, they were continually observed for any signs of toxicity. Form B (per 8 (a)* for Submission of Research Protocol Application for Permission for Animal Experiments was approved by the Institutional Animal Ethics Committee (IAEC) and submitted to CPCSEA, New Delhi, before the commencement of the study. Approved under approval number XXVIII/MSRFPH/COL/PG-06/November 15, 2023 by the Institutional Animal Ethics Committee of the Department of Pharmacology, Faculty of Pharmacy, M.S. Ramaiah University of Applied Sciences, the study protocol was approved during a meeting on November 15th, 2023. Standard laboratory conditions were used for the maintenance of Wistar rats (180–250g), with each group containing 6 animals of both sex [42]. Following an acclimatization period of seven days, the animals were randomized to the Sub-acute toxicity groups. The animals had unlimited access to water and a normal pellet diet. The regulated laboratory settings they were kept in included 12 h of light and dark cycles, 22 ± 2 °C

temperatures, and 45–60 % humidity. The FA-FeA-SWCNTs formulation is given orally to the animals seven days a week for a total of 28 days, with 0.7 mg/kg as the low dosage, 1.5 mg/kg as the mid-dose, and 3 mg/kg as the high dose. A satellite group is monitored for an additional 14 days without treatment. For 28 days, they were observed twice a day (at 9:00 a.m. and 4:00 p.m.) for behavioral anomalies, toxicity symptoms, and mortality. From the start of the trial, changes in food and water consumption and body weight were observed. On the 28th day, every rat was kept starving all night. On the 29th day the animals were sacrificed, for hematological and biochemical studies, cardiac punctures were used to obtain blood samples. This was followed by histopathological studies [43].

3.5.1. Evaluation parameters

At the end of the sub-acute toxicity study on the 29th day, all the animals were fasted overnight, weighed and sacrificed. Blood samples were collected via cardiac puncture for hematological analyses (including RBC, Hb, PCV, and platelet count) and biochemical analyses (including SGOT, SGPT, ALP, Total Bilirubin, Total protein, Uric acid, BUN, Serum creatine, Uric acid, Sodium, Potassium) [44]. Necropsy was performed and internal organs (liver, heart, kidney, uterus, spleen, brain, lungs, stomach, pancreas, testis, skin, spinal cord, and breast) were weighed and fixed in 10 % buffered formalin for histopathological examination. Data were expressed as mean ± SEM, with one-way ANOVA followed by a *t*-test performed using SPSS, considering differences statistically significant at $p \leq 0.05$.

3.5.2. Tumor induction

Six groups of six animals each were created from thirty-six female Wistar rats. A single dosage of DMBA (20 mg/rat) suspended in 0.7 mL of almond oil, the prepared inducing agent was then subcutaneously injected under the breast tissue of the animal in any one of the 6 pairs of mammary glands of the rat for the induction of breast cancer, and the animals were observed for 7–10 days afterward and the tumor was measured with a vernier caliper [45]. The temperature-controlled room was used throughout the experiment, and exposure to light and darkness was kept for 12 h, respectively.

3.5.3. Study design for in vivo studies

Six groups of rats were randomly grouped for treatment for 21 days, as shown in Supplementary Table 1. Animals were administered the formulation orally seven times a week at a low dose of 0.7 mg/kg, a mid-dose of 1.5 mg/kg, and a high dose of 3 mg/kg [46]. Following therapy, blood samples were collected and subjected to hematological parameters such as the Complete Blood Cell Count, Liver Function Test, and Renal Function Test. Antioxidant levels were also assessed. Histopathological analysis was used to examine the formulation's impact on breast tissue.

3.5.4. Evaluation of tumor size

A vernier caliper was used to obtain accurate millimeters (mm^3) measurements to assess the volume of tumors in Wistar rats. The scale was used to measure the shortest and longest tumor diameters.

$$\text{Tumor volume } \left(mm^3\right) = \frac{d^2 \times D}{2}$$

Where d and D are the shortest and longest diameter in mm, respectively [45].

3.5.5. Estimation of hematological parameters

Animals in all groups that had been fasting all night were weighed at the end of the study and sacrificed. A cardiac puncture took 10 mL of blood from animals in all groups, and 3 mL was transferred into K2EDTA, an anticoagulant for hematological analyses, including RBC (Red blood cell), Hb (Hemoglobin), PCV (Packed-Cell Volume), and platelet count, and all blood samples were labelled immediately [46].

3.5.6. Estimation of biochemical parameters

7 mL of collected blood was transferred into a heparin coagulant tube and was allowed to clot for 30 min before being subjected to centrifugation for serum separation. Biochemical analyses include SGOT, SGPT, ALP, Total bilirubin, Total protein, Uric acid, BUN, Serum creatine, Uric acid, Sodium, and Potassium [44].

3.5.7. Evaluation of antioxidant parameters in breast tissue

During the surgical resection, tumor tissue was removed and wiped with filter paper to clean it. The tissue was then divided into two halves. One-half was utilized for antioxidant parameters. The tissue samples were sliced into small pieces to prepare the tissue homogenate and lysate for analysis. The samples were processed in an ice-cold 0.1M tris-HCl buffer at pH 7.4. The tissue sample mixture was spun for 15 min at 10,000 rpm to collect the supernatant solution [47]. The supernatant from the centrifuge homogenate was utilized for SOD (superoxide dismutase), Catalase, and Glutathione assays.

3.5.8. Histopathological studies

All of the animals in the test and control groups' rats were sacrificed on the 29th day of the study, and blood samples were taken through cardiac puncture. A gross examination of the breast tissue and a necropsy was done. Subsequently, every internal organ was removed, cleared of fat, weighed, and examined under a microscope. Additionally, relative organ weight was computed. Finally, they were preserved for histological analysis in a 10 % buffered formalin solution [48].

3.6. Statistical analysis

Standard Error of Mean (SEM) represented all qualitative data as mean ± SEM. Using SPSS software, a one-way analysis of variance (ANOVA) and a *t*-test were used for each statistical study. Statistically significant differences were accepted at $p \leq 0.05$.

4. Results

4.1. Molecular modelling studies

The molecular docking study was performed to evaluate the binding efficiency of ferulic acid against standard drugs for different protein targets. For Abl Kinase, with PDB ID 2HZI, the standard drug imatinib showed an excellent docking score of −14.4 kcal/mol by interacting at MET-318 and LYS-271. Ferulic acid had a docking score of −6.8 kcal/mol but had additional interactions at GLU-316 and TYR-253, which could indicate an alternative binding mode. For the Renin Complex PDB ID 3VUC, aliskiren had a very good binding affinity with a docking score of −12.62 kcal/mol by interacting at PRO-306, GLY-228, PHE-124, and ASP-226. Ferulic acid had a lower score than that (−3.5 kcal/mol) but interacted with SER-84, TYR-83, and ASN-43 under limited potential for binding. For the VEGF receptor PDB ID 3WZE, the standard drug bevacizumab produced a docking score of −8.15 kcal/mol by forming interactions at CYS-919, ASP1046, and GLU885. In contrast, ferulic acid scored −7.45 kcal/mol by forming interactions at ASP1046 and GLU917, indicating almost similar binding affinity. For Progesterone Receptor PDB ID 3ZR7., the standard ligand progesterone produced a docking score of −6.7 kcal/mol by binding at GLN725., TYR890., and PHE778, while ferulic acid scored −6.5 Kcal/Mol due to interactions at GLN725., ARG766., AND ASN719 equivalent binding behavior. In the KEAP1 receptor (PDB ID: 5GIT), no standard drug was available for ferulic acid, but it showed a docking score of −3.9 kcal/mol instead of interaction potential with ARG-135 and HIE-129 compared with standard drugs in other targets. For the estrogen Receptor (PDB ID: 5WGD), tamoxifen scored −11.4 kcal/mol, which interacted with ARG-394, GLU-353, PHE-404, and HIE-524 while ferulic acid scored −6.4 kcal/

mol, which interacted with ARG-394, PHE-404, and LEU-387. In the case of Mitogen-Activated Protein Kinase (PDB ID: 6E2N), trametinib had a docking score of −8.06 kcal/mol interacting with LYS-709 and VAL-757. In comparison, ferulic acid had a marginally lower score of −7.6 kcal/mol but provided an additional interaction with ASP-822 indicating strong binding potential. For the Tubulin Alpha receptor (PDB ID: 6S8L), paclitaxel had very low docking scores at −2.4 kcal/mol due to interactions at SER241 and VAL238 as compared to stronger binding by ferulic acid at −4.8 kcal/mol due to interactions at TYR202, GLH200, and THR317.

For the Human Glyoxalase 1 Receptor, PDB ID: 7WT0, ferulic acid gave a docking score of −2.6 kcal/mol with no standard drug available for comparison. Lastly, for the Epidermal Growth Factor Receptor, PDB ID: 8A27, erlotinib had a score of −6.05 kcal/mol binding to ASP-855, PHE-856, LEU-858, GLY-857, and LYS-745 whereas ferulic acid had a slightly lower score of −5.9 kcal/mol only interacting with ASP-855, according to the molecular docking studies. KEAP1, Mitogen-Activated Protein Kinase 1, and Human Glyoxalase 1 Receptor were shown to have higher binding interactions with ferulic acid, as shown in Table 1 and Fig. 2. These interactions shared similarities in amino acid composition with the standard drug utilized in this study.

The ADMET properties of ferulic acid were evaluated using pkCSM software. Ferulic acid showed moderate solubility in water with a log mol/L value of −2.909 and exhibited quite poor CaCo2 permeability, log Papp = 0.195, suggesting some difficulties in transcellular absorption. However, its high intestinal absorption of 93.22 % indicates efficient uptake in the gastrointestinal tract, while its skin permeability (log Kp = −2.722) suggests potential applicability in transdermal delivery systems. The distribution properties revealed a quite limited volume of distribution in humans VDss = −1.098 log L/kg with moderate plasma protein binding Fu = 0.472 hence facilitating its systemic availability. On the other hand, ferulic acid exhibited poor permeability across the blood-brain barrier log BB = −0.28 and central nervous system CNS; log PS = −2.535; thus, it was not prospective as a CNS-active agent.

The compound was neither predicted nor exhibited inhibition of CYP1A2 or CYP2C19. Thus, it has a reduced risk of metabolic drug-drug interaction. Excretion studies have shown total clearance of 0.619 log ml/min/kg, efficient elimination and also not a substrate for renal OCT2, hence the risk of renal toxicity is avoided. Toxicity predictions were favorable with ferulic acid found to be non-toxic in the Ames test with no mutagenic potential identified. The MTD for humans was extrapolated to be 1.444 log mg/kg/day and not classified as a hERG I or II inhibitor; hence, cardiac toxicity is minimal, if any. Acute oral toxicity in rats is 2.322 mol/kg, and chronic oral toxicity is 1.794 log mg/kg/bw/day. Ferulic acid also showed non-hepatotoxic, non-sensitizing to skin and low aquatic toxicity as demonstrated by low toxicity against *Tetrahymena pyriformis* and minnows.

Overall, ferulic acid showed a promising ADMET profile with good intestinal absorption, low toxicity and a low probability of metabolic or renal drug interactions. On the other hand, its poor permeability at biological barriers like $CaCO_2$ cells and the blood-brain barrier points out possible zones for structural alteration aimed at enhancing bioavailability and widening therapeutic use. These findings reinforce the notion that ferulic acid has potential as a safe and effective candidate for further pharmacological exploration, the results were shown in Supplementary Table 2.

Initially, MD simulation was carried out for a time period of 100ns for the ferulic acid complex with KEAP1, Mitogen Activated Protein Kinase 1 and Human Glyoxalase 1. Based on the initial screening, only MAPK (6E2N) showed lower RMSD and retained its stability. Hence, it was extended for a period of 1000ns.

The MD simulation of the protein-ligand complex for the target protein MAPK was carried out for 1000 ns under physiological conditions, thus elucidating the system's structural robustness, molecular flexibility, and interaction kinetics. RMSD analysis corresponds to the general stability of the system; fluctuations in protein RMSD remained between 1 and 3 Å throughout the simulation period. Since it remained stable along with the protein backbone, the ligand stayed bound in its active site, corroborating the docking results' validity. The RMSF analysis revealed specific flexible protein regions; loops and terminal regions showed peaks that naturally are more flexible than those in secondary structure components like α-helices and β-strands. Most importantly, there was minimal fluctuation among residues within the binding pocket, indicating stable interactions between ligand and protein.

The interaction analysis revealed hydrogen bonds as the most important contributors to binding stability, which was observed uniformly throughout the simulation. Additional interactions like hydrophobic contacts, ionic bonds, and water-mediated bridges added further stability to the protein-ligand complex. Key residues LYS-709 and VAL-757 were identified as crucial for binding with stable hydrogen bonds and hydrophobic interactions. Water-mediated interactions bridged the ligand and adjacent residues, adding to the complex's stability. The low RMSF values of the ligand conformed to its stability and fluctuated very little, particularly for functional groups that were essential for binding. Analysis of the torsional profiles confirmed that there was low strain in the rotatable bonds of the ligand allowing it to bind conformationally well within the active site. The results were shown in Fig. 3.

Overall, the MD simulation affirmed the structural stability and

Table 1
Molecular docking scores of Ferulic acid with various breast cancer targets.

SL. No	Protein Name	PDB ID's	Standard Drug	Standard Score (Kcal mol^{-1})	Standard Binding Amino Acid	Ferulic Acid Score (Kcal mol^{-1})	Ferulic Acid Binding Amino Acid
1	Abl Kinase	2HZI	Imatinib	−14.4	MET-318, LYS-271	−6.8	MET-318, LYS-271, GLU-316, TYR-253
2	Renin Complex	3VUC	Aliskiren	−12.62	PRO-306 GLY-228, PHE-124, ASP-226	−3.5	SER-84, TYR-83, ASN-43
3	VEGF Receptor	3WZE	Bevacizumab	−8.15	CYS-919, ASP-1046, GLU-885	−7.45	ASP-1046, GLU-917
4	Progesterone Receptor	3ZR7	Progesterone	−6.7	GLN-725, TYR-890, PHE-778	−6.5	GLN-725, ARG-766, ASN-719
5	**KEAP1 (Kelch-like ECH-associated Protein 1)**	**5GIT**	**Co-crystal**	**−3.4**	**ASP-87, ALA-88**	**−3.9**	**ARG-135, HIE-129**
6	Oestrogen Receptor	5WGD	Tamoxifen	−11.4	ARG-394, GLU-353, PHE-404, HIE-524	−6.4	ARG-394, PHE-404, LEU-387
7	**Mitogen-Activated Protein Kinase (MAPK)**	**6E2N**	**Trametinib**	**−8.06**	**LYS-709, VAL-757**	**−7.6**	**LYS- 709, VAL-757, ASP-822**
8	Tubulin Alpha Receptor	6S8L	Paclitaxel	−2.4	SER-241, VAL-238	−4.8	TYR-202, GLH-200, THR-317
9	**Human Glyoxalase 1 Receptor**	**7WT0**	**Co-crystal**	**−1.6**	**MET-157**	**−2.6**	**MET-157, LYS- 156**
10	Epidermal Growth Factor Receptor	8A27	Erlotinib	−6.05	ASP-855, PHE-856, LEU-858, GLY-857, LYS-745	−5.9	ASP-855

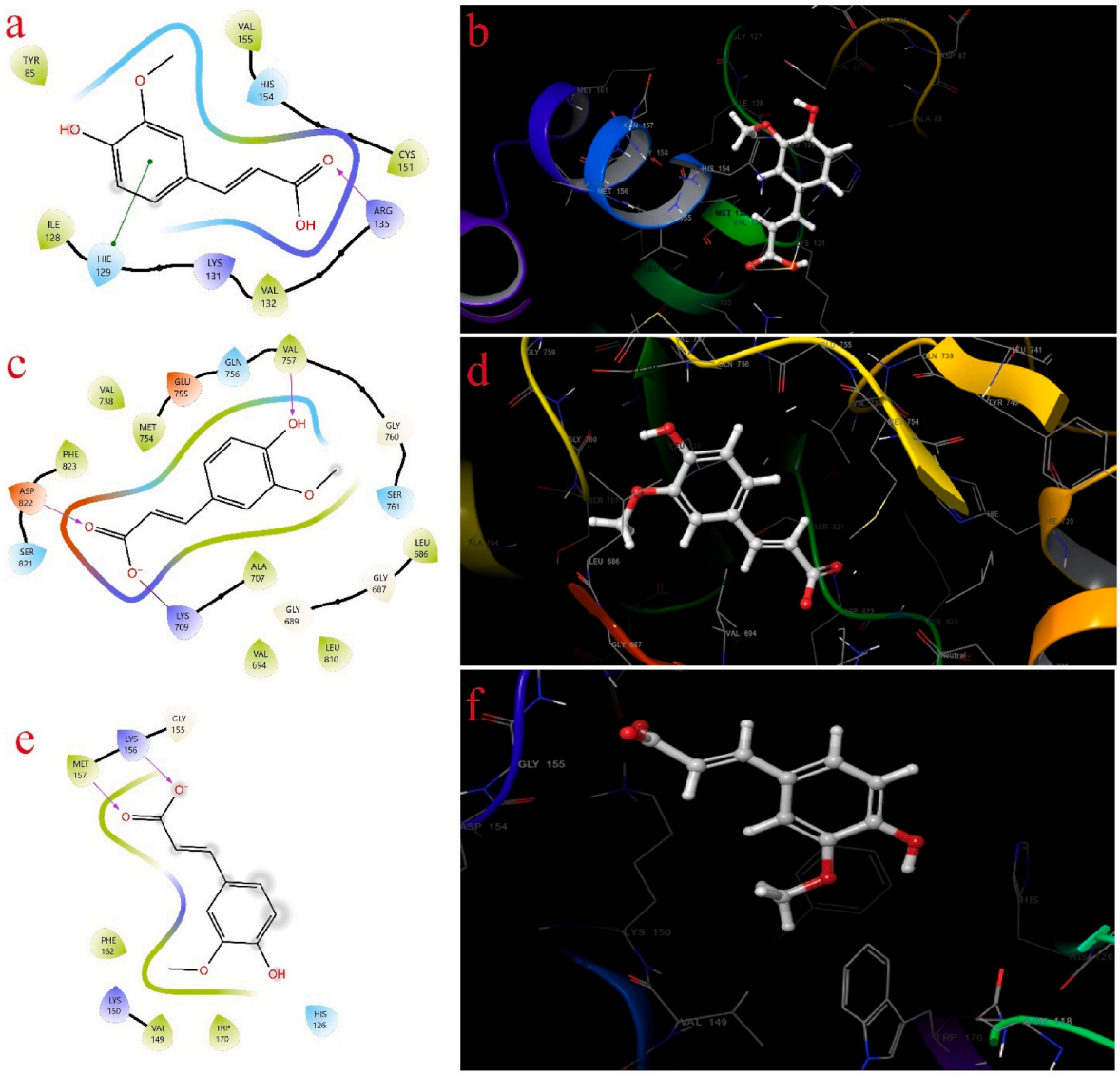

Fig. 2. Molecular docking scores of Ferulic acid with various targets of breast cancer. (a, b: 2D and 3D of Ferulic Acid-KEAP1 complex; c, d: 2D and 3D of Ferulic Acid-MAPK complex; e, f: 2D and 3D of Ferulic Acid-HG1R complex.)

favorable binding characteristics of the protein-ligand complex. Results will emphasize not only the strong and stable interactions between the ligand and important residues at the binding site but also its potential further as a promising candidate for optimization in drug development. The stable RMSD, controlled RMSF, and continuous interactions all corroborate the binding mode and confirm the validity of the simulation results.

In conclusion, the MAPK complex has been identified as a possible target for ferulic acid in the therapy of breast cancer attributed to the combination of molecular docking, ADMET and MD simulations.

4.2. Formulation of FA_FeA_SWCNTs

Using UV–visible spectrophotometry, the synthesis of FA-NHS was first confirmed. This is a simple method to confirm structural alterations and establish the formation of a complex between the γ-carboxylic group of FA and the amino group of N-Hydroxy succinimide using UV visible absorption peak analysis. NHS is showing a slight peak due to n→π* transition. The UV–visible spectrum of the mixture has exhibited a subtle shift to a lower wavelength, indicating a hypsochromic shift. This hypsochromic shift suggests that an interaction has occurred between FA and NHS. Additionally, one of the NHS's peaks has broadened, which indicates the compound's encapsulation or molecular interaction. The OH groups of FA in the crystalline structures are linked to the peaks at 3590 cm^{-1}, 3496 cm^{-1}, and 3330 cm^{-1}, shown in Supplementary Fig. 1a. Furthermore, the OH groups of glutamic acid are responsible for distinctive peaks of folic acid in the wide band between 3101 cm^{-1} and 2400 cm^{-1}. The (C=N) stretching peaks at 1635 cm^{-1} and 1597 cm^{-1} are associated with the bending of (CONH2), whereas the (C=C) stretching of the phenyl and pterin rings are associated with the peak at 1477 cm^{-1}. These interactions suggest that FA has structurally changed to form FA-NHS. Characteristics bands at 1626, 2928, and 1199 cm^{-1} of NHS in Supplementary Fig. 1b were identified as the stretching forms of aromatic C=C bending, carboxylic acid C=O and O-H stretch unconjugated, and primary aliphatic amine N-H stretching, respectively. Two significant absorption peaks are seen in Supplementary Fig. 1c of FA-NHS at 1660 cm^{-1} because of the N-O bond and 1700 cm^{-1} because of the C=O bond. This occurrence demonstrates the successful transition of FA into FA-NHS.

The solvent deposition was used to develop ferulic acid encapsulated folic acid conjugated single-walled carbon nanotube. Folic acid's linkage to SWCNTs enables the nanotube formulation to bind with a high

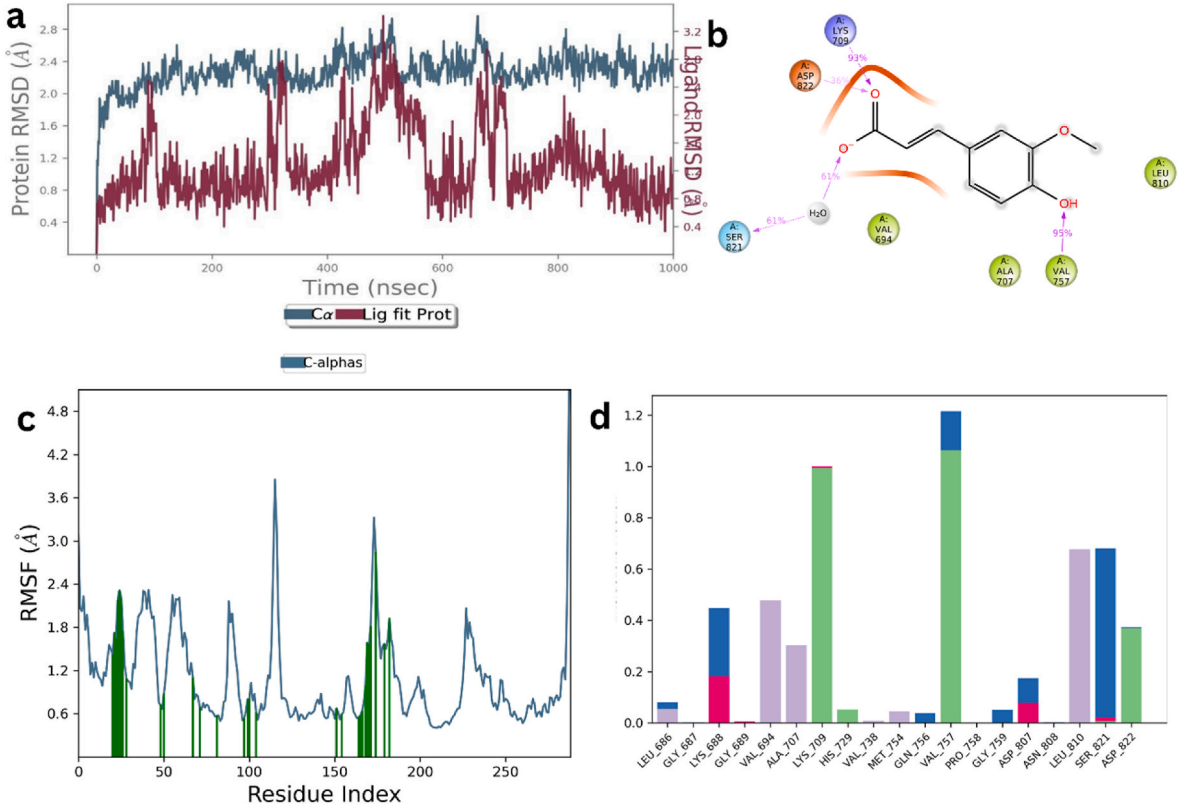

Fig. 3. Molecular dynamics simulation interactions of Ferulic acid - MAPK protein complex: a) RMSD; b) 2D interactions; c) RMSF; d) Protein-Ligand interactions.

affinity for targeted medication administration and therapeutic applications to folate receptor that increases on the surface of cancer cells. Our previous study's finding showed that myricetin-loaded bovine serum albumin nanoparticles conjugated with folic acid had the ability to strengthen the chemotherapeutic drug myricetin for its anticancer effects. Furthermore, the SWCNTs can be coupled to folic acid, which targets a variety of cancers, to deliver doxorubicin to the cancer cells with considerably better efficiency than free doxorubicin. It has been demonstrated that doxorubicin delivered from the improved carbon nanotubes damages nuclear DNA and prevents cell division. The amount of ferulic acid was measured using absorbance measurements at different time intervals to confirm that it was encapsulated in the SWCNTs and nanoformulation. The formation of FA-FeA-SWCNTs is an outcome of Ferulic Acid gradually encasing itself within SWCNTs, as seen in Supplementary Fig. 2. The results showed that the EE%, or the amount of Ferulic acid entrapped in SWCNTs, was 75.432 ± 2.42 %. Ferulic acid's LC% in SWCNTs was found to be 8.584 ± 1.581 % and Folic Acid LC% was found to be 84.357 ± 1.47 %.

4.3. Characterization of FA-FeA-SWCNTs

The structure of Ferulic Acid is confirmed by the IR spectra, which show peaks at 3434 cm^{-1} (carboxylic acid O-H stretching), 2917 cm^{-1} (C-H bond stretching), 1313 and 1024 cm^{-1} (carboxylic acid C-O), 1247 and 1290 cm^{-1} (C-C stretching vibrations),1024 cm^{-1} (aromatic C=C), 954 and 856 cm^{-1} (C-H bending of aromatic ring) shows that natural ferulic acid has not undergone significant chemical alterations. However, the absence of specific peaks in the FA-FeA-SWCNTs formulation indicates compatibility and structural integrity for targeted drug administration. For the carboxylate SWCNT, the band resulting in the C=O stretching is visible in the range of 2900 cm^{-1}, and the prominent peak can identify the acid-carbonyl stretching at 1506 cm^{-1}. The characteristics of FAs carboxylic acid hydroxyl stretching appear in the distinctive peak at 3424 cm^{-1} in the FTIR spectra shown in Supplementary Fig. 3 of FA-FeA-SWCNTs.

The nano formulation's particle size was determined to be 36.6 nm, falling within the normal range for drug-delivery nanoparticles, Fig. 4a. Due to their increased surface-to-volume ratio and capacity to interact with biological systems, smaller particles are favorable in terms of improving the formulation's bioavailability and therapeutic effectiveness.

The zeta potential was −7.84 mV, and it was extremely stable. That negative number means there is electrostatic attraction, so the particles don't lump together, keeping them stable over time, shown in Fig. 4b. The formulation of FA-FeA-SWCNTs was analyzed by XRD; the formula was amorphous, as shown in Supplementary Fig. 4. Because they are more soluble and have more surface area, amorphous compounds dissolve and are more bioavailable. We can tell that the FA-FeA-SWCNTs are amorphous from the absence of crystal peaking on the XRD. Here are some of the very pure and homogeneous single-walled carbon nanotubes (SWCNTs) in this SEM image, shown in Fig. 4c. These were long, skinny, zero-defect cylinders, 1–2 nm across and they were flat. Such properties exhibit SWCNTs' mechanical stability and stiffness for applications ranging from general-purpose to their distinctive form and large surface area.

4.4. In vitro drug release

Ferulic acid release from FA-FeA-SWCNTs has been studied at 37 ± 2 °C in phosphate buffer (pH 7.4) and acetate buffered system (pH 3.4 and pH 5.4). The cumulative percentage of FA released over time illustrates it's *in vitro* release in Supplementary Fig. 5. Using UV–visible spectrometry, the amount of FA release was quantified. The FA-FeA-SWCNTs formulation released a cumulative quantity of ferulic acid after 30 h of incubation, which was 35.5 ± 2.60 % (pH 3.5), 31.2 ± 2.58 (pH 5.5), and 32.7 ± 2.47 % (pH 7.2). The result showed Ferulic acid's continuous and sustained release behavior would sustain the drug's concentration. This gradual release helps to maintain therapeutic levels

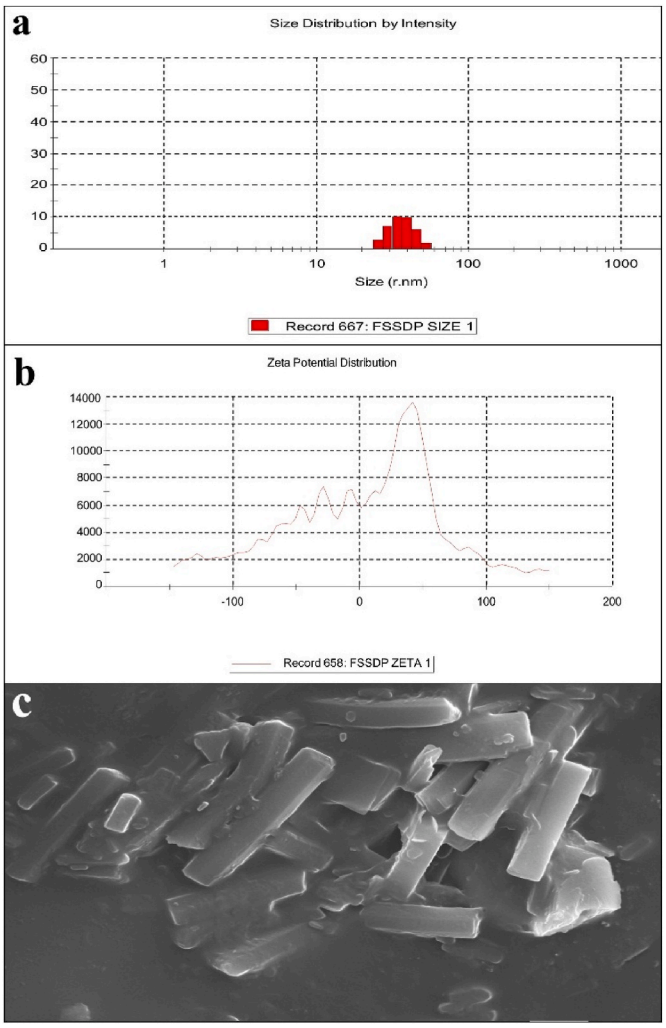

Fig. 4. a) Particle Size Analysis of FA-FeA-SWCNTs; **b)** Zeta Potential of FA-FeA-SWCNTs; **c)** SEM image of FA-FeA-SWCNTs.

over time and improves the overall convenience of the therapy.

4.5. *In vitro cytotoxicity assay*

4.5.1. *MCF-7 cellular viability*

Using the calorimetric MTT assay, the cellular viability of the formulated FA-FeA-SWCNTs was examined on MCF 7 cell lines, indicating a substantial reduction in cell viability. Different quantities of FA-FeA-SWCNTs (100, 50, 25 μg/mL), doxorubicin (25 μg/mL), and free ferulic acid (100 μg/mL) were introduced to MCF-7 cells. The % of cellular survival of MCF-7 cells is shown in Fig. 5. The findings indicated that, compared to the control, the treatment of FA-FeA-SWCNTs resulted in a concentration-dependent reduction in cell viability. The formulation's IC_{50} value was found to be 19.60 μg/mL, indicating that this dose is sufficient to cause a 50 % reduction in cancer cell viability. Given that this result is closer to the IC_{50} value of Doxorubicin, a well-known chemotherapeutic medication, it suggests that the formulation may have cytotoxic properties similar to that drug. Fig. 6 represent dose response curve for cytotoxicity.

4.5.2. *Analysis of apoptosis using AO/EB staining*

This work investigated the apoptosis-inducing capacity of FA-FeA-SWCNTs in MCF-7 cells by fluorescence microscopy and the AO/EB dual staining assay. After 48 h of treatment with FA-FeA-SWCNTs, MCF-

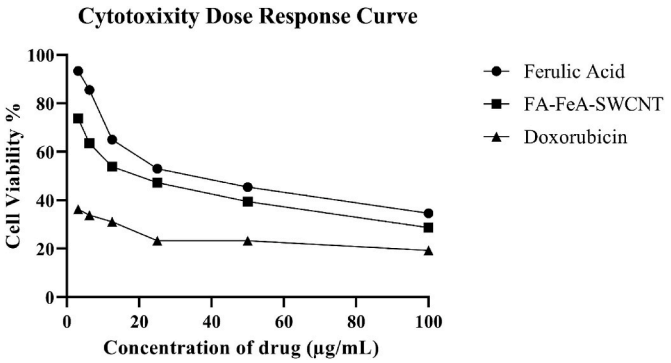

Fig. 6. Dose response curve for cytotoxicity.

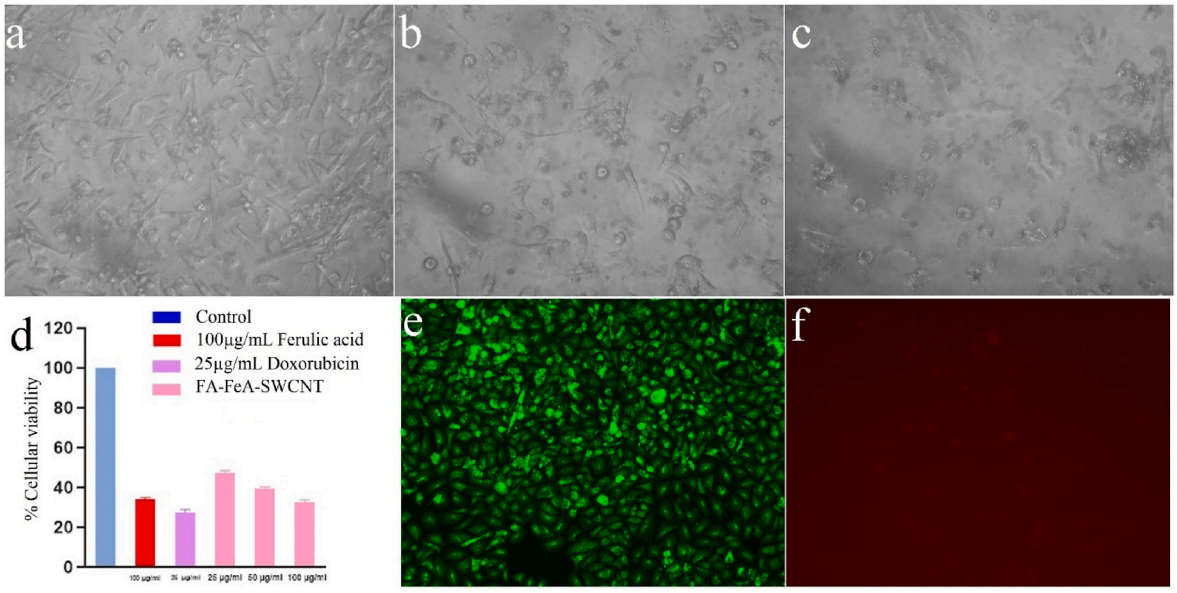

Fig. 5. *In vitro* MTT assay of FA-FeA-SWCNTs: a) MCF-7 cell lines treated with DMSO; b) FA-FeA-SWCNTs in MCF-7 cell lines at 100 μL; c) Doxorubicin in MCF-7 cell lines at 100 μL; d) % cell viability; e) AO/EB staining existence of viable cells; f) AO/EB staining post apoptosis.

cell morphological changes were examined at the IC_{50} concentration. CA-Kaf NPs-treated cells displayed characteristic apoptotic features, including cytoplasmic contraction and membrane blebbing. Upon binding to DNA, AO emitted a vivid green fluorescence, signifying the existence of viable cells (Fig. 5e). Following 48 h of treatment, the ligation of EB to the denatured DNA produced a reddish-orange colouration. This modification differentiates the later stages of apoptosis (Fig. 5f). Only cells exhibiting compromised membrane integrity were stained with EB. The findings indicated that FA-FeA-SWCNTs compromised the integrity of the cell membrane. The studies showed that CA-Kaf NPs may induce apoptosis-mediated cell death in MCF-7 cells.

4.6. CAM assay

The FA-FeA-SWCNTs formulation was evaluated at three different dose levels: 12 μg/mL (high dose), 6 μg/mL (mid dose) and 3 μg/mL (low dose) shown in Fig. 7. Treatment doses were compared to a standard doxorubicin group (0.1 mL) and a control group (normal saline). All results displayed a dose-dependent anti-neovascularization inhibition, with the highest dose (12 μg/mL) showing the most significant anti-angiogenic effect. At this optimized dose level, the FA-FeA-SWCNTs formulation achieved a strong 71.2 % blockade in neovascularization compared to a 60.3 % blockade observed with standardized doxorubicin treatment illustrated in Supplementary Table 3. FA-FeA-SWCNTs formulation to inhibit neovascularization is a strong candidate for being a potent anti-neovascularization agent through anti-angiogenic activity. Fig. 8 represents Dose Response Curve for anti-angiogenesis studies. The FA-FeA-SWCNTs formulation can prevent new blood vessel formation, starving tumors for nutrients and reducing physical oxygen consumption, ultimately slowing the development of cancer.

4.7. In vivo toxicity studies

4.7.1. General sign and behavioral analysis

The sub-acute oral toxicity studies during the experiment indicated no mortality due to the treatment in either sex of the rats upon oral administration of FA-FeA-SWCNTs. During the duration of this investigation, physical observation of rats treated with the formulation for subacute oral toxicity test revealed that none of them displayed any symptoms of toxic effects, including abnormalities in skin and hair, eyes and mucous membranes, behavioral patterns, tremors, salivation, diarrhea and coma. All animals in every group showed no microscopic or gross pathological abnormalities, confirming that the formulation is harmless for animal health even at the high dose levels utilized in this study.

4.7.2. Effect of FA-FeA-SWCNTs intake on food and water intake, body weight and organ weight

Throughout the duration of the study, there was no noticeable difference in the food and water intake of the FA-FeA-SWCNTs treated group from that of the control group. The body weight of the control and FA-FeA-SWCNTs treated groups increased gradually reflected in Supplementary Table 4. When compared to the control animals, the percentage changes in body weight of the FA-FeA-SWCNTs treated groups were not statistically different ($P > 0.05$). As shown in Supplementary Table 5, the organ weights of the control and formulation-treated groups did not vary statically.

4.7.3. Effect of FA-FeA-SWCNTs on hematological and biochemical parameters

The biochemical profile of male and female rats wasn't altered by the 28-day treatment with FA-FeA-SWCNTs, as indicated in Table 2. Likewise, treatment with formulation did not change the hematological profile of rats. All values in the control and treatment groups in the hematological and biochemical tests were within the reference range. During a 28-day subacute toxicity assessment, a favorable safety profile

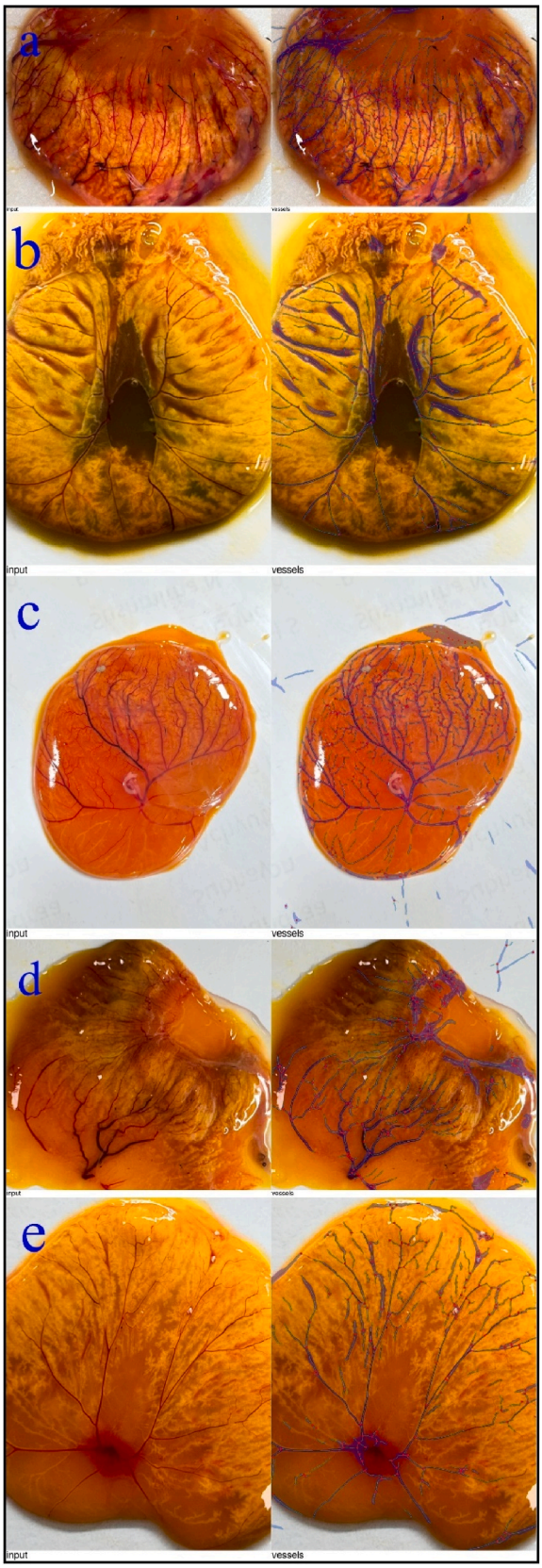

Fig. 7. Anti-angiogenesis activity of FA-FeA-SWCNTs (Inhibition of neovascularization: a) Normal control; b) Standard drug; c) Low dose (3 μg/mL); d) Mid dose (6 μg/mL); e) High dose (12 μg/mL).

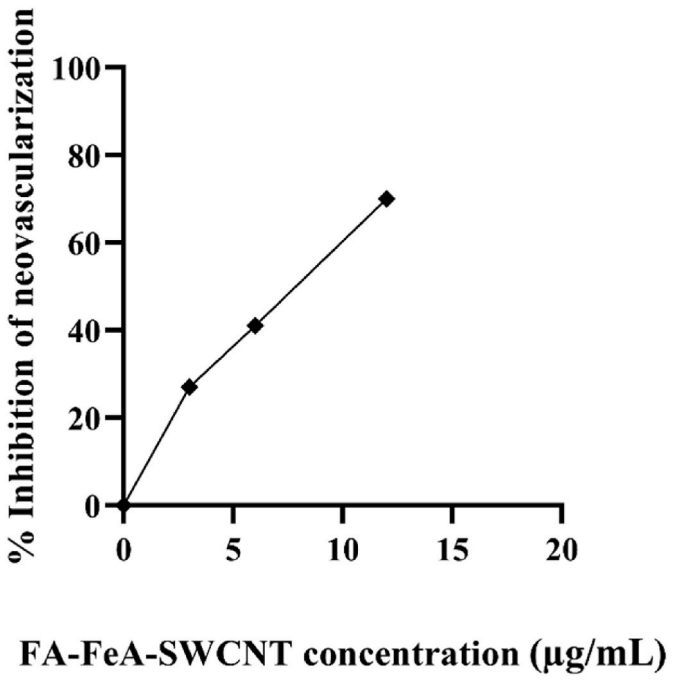

Fig. 8. Dose response curve for neovascularization.

Table 2
Subacute biochemical profile of male and female rats treated with FA-FeA-SWCNTs.

Parameters	Normal Range	Low Dose	Mid Dose	High Dose
Haematological Parameters				
Haemoglobin (g/dL)	8.6–15.38	15.10 ± 0.15	15.27 ± 0.39	16.5 ± 0.18
RBC (× 10^6/µL)	4.75–6.8	7.33 ± 0.27	7.50 ± 0.15	7.5 ± 0.19
PCV (%)	10.0–47.0	35.93 ± 0.94	38.87 ± 1.13	42.2 ± 1.73
Platelet Count (cells/mm^3)	1.48–6.15	8.04 ± 0.18	8.30 ± 0.10	8.37 ± 0.09
Liver Function Test				
Total Protein (g/dL)	6.3–7.3	6.47 ± 0.15	6.53 ± 0.20	8.27 ± 0.12
Albumin (gm %)	3.1–4.6	2.21 ± 0.06	2.20 ± 0.12	2.55 ± 0.08
Globulin (gm %)	3.5–5.3	5.9 ± 0.06	4.20 ± 0.12	3.87 ± 0.37
SGOT (µ/L)	34–109	173.70 ± 1.69	152.50 ± 1.21	160.5 ± 1.45
SGPT (µ/L)	13–56	72.07 ± 1.00	69.33 ± 0.64	80.60 ± 0.64
ALP (IU/L)	95–611	177.00 ± 1.69	225.70 ± 1.76	203.50 ± 1.11
Total Bilirubin (mg/dL)	0.2–0.7	0.18 ± 0.01	0.13 ± 0.01	0.20 ± 0.01
GGT (U/L)	0.5–5.3	1.72 ± 0.10	3.45 ± 0.09	2.77 ± 0.06
Kidney Function test				
Uric Acid (mg/dL)	0.6–1.45	1.46 ± 0.01	1.30 ± 0.03	1.49 ± 0.02
Urea (mg/dL)	15–30	30.13 ± 1.21	32.80 ± 0.72	35.43 ± 1.55
BUN (mg/dL)	12.3–77.6	15.63 ± 0.45	15.53 ± 0.52	16.27 ± 0.52
Serum Creatinine (mg/dL)	0.2–0.7	0.84 ± 0.01	0.84 ± 0.01	0.94 ± 0.01
Sodium (mmol/L)	138–155	134.70 ± 0.67	135.70 ± 1.31	134.70 ± 1.09
Potassium (mmol/L)	4.6–6.0	4.67 ± 0.09	4.70 ± 0.12	4.67 ± 0.09
Chlorides (mmol/L)	100–110	97.73 ± 2.13	99.50 ± 1.58	97.73 ± 2.29

Values are expressed as Mean ± SEM where n = 3; One way ANOVA followed by a comparison between disease vs treatment groups using Dunnett's *t*-test, where a = $p < 0.05$, b = $p < 0.01$, c < 0.001 and d = $p < 0.0001$.

for the FA-FeA-SWCNTs formulation was discovered across all evaluated parameters. According to measurements of antioxidant levels, the formulation did not adversely affect the body's defenses against oxidative stress; in particular, it may have enhanced them. The complete blood count (CBC) results, which showed no noticeable changes in hemoglobin levels, platelet counts, or red and white blood cell counts, demonstrated that the formulation did not cause hepatotoxicity. The serum liver profile (LFT) and serum renal profile (RFT) also showed normal enzyme levels and metabolic indicators. This suggests that administering FA-FeA-SWCNTs at low, mid, and high doses did not result in hepatotoxicity and nephrotoxicity.

4.7.4. Morphological analysis

FA-FeA-SWCNTs treatment exhibited no effect on the relative weight. Compared to the control group, the macroscopic examination of treated animals' target organs revealed no significant changes in colour or texture. In addition, all organs examined by microscopy did not show any histological changes as demonstrated in Fig. 9.

4.7.5. Histopathological report of target organs on FA-FeA-SWCNTs

The formulation elicited dose-related organ responses and toxicity based on histopathology findings. The animals underwent histological examination in low, mid, and high-dose groups. A more complicated picture was provided by the high-dose group, where little distention of the sinusoidal spaces of the liver is a sign of potential hepatic stress. Meanwhile, the kidneys, lungs, and heart remained within their normal shapes. Noteworthy active proliferations were also established in the pancreas and testis. Hormone effects may be those parts of the medication. Therefore, it may be presumed that the high dose could elicit some physiological systems. Moderate congestion and ulceration aside, it was accompanied by a high dose-related beneficial response based on overall histopathology. The pancreas, spleen, uterus, and testis showed active proliferative changes, which may be an adaptive or compensatory response to the formulation. This highlights the need for further investigation into the underlying mechanisms.

4.8. In vivo anti-cancer studies

4.8.1. Body weight

Based on our experimental findings, the tumor-induced (DMBA) group's body weight decreased soon compared to the normal control group rats. The animal's persistent decrease in body weight throughout the study is an indirect sign of disease, with the weight loss attributed to increased lipolysis and proteolysis caused by the presence of breast tumors. It was noted that, compared to rats in the disease group, all treatment group animals first showed a decrease in body weight, followed by a gradual increase. The final body weight (g), body weight gain/loss (g), food intake (g/day), and food efficiency (body weight gain (g/day)/food intake) remained satisfactory in all the experimental groups, revealed no signs of toxicity and cachexia.

4.8.2. Animal tumor size

Tumor size increased progressively with time in the disease control group and reached 36.00 ± 0.56 mm by Day 28, indicating the aggressive nature of DMBA-induced carcinogenesis. Doxorubicin at 4 mg/kg and high-dose treatment at 3 mg/kg efficiently arrested tumor growth, reducing sizes to 4.12 ± 0.02 mm by Day 28. Mid-dose treatment at 1.5 mg/kg significantly reduced the tumor size to 6.56 ± 0.032 mm compared to low-dose treatment at 0.7 mg/kg, which reduced the tumor size to 8.25 ± 0.027 mm, as shown in Supplementary Table 6. These results prove a dose-dependent anti-tumor effect, with the high dose being as effective as doxorubicin. These findings thereby allow the consideration of this treatment as a potentially effective alternative to DMBA-induced carcinogenesis, warranting further study.

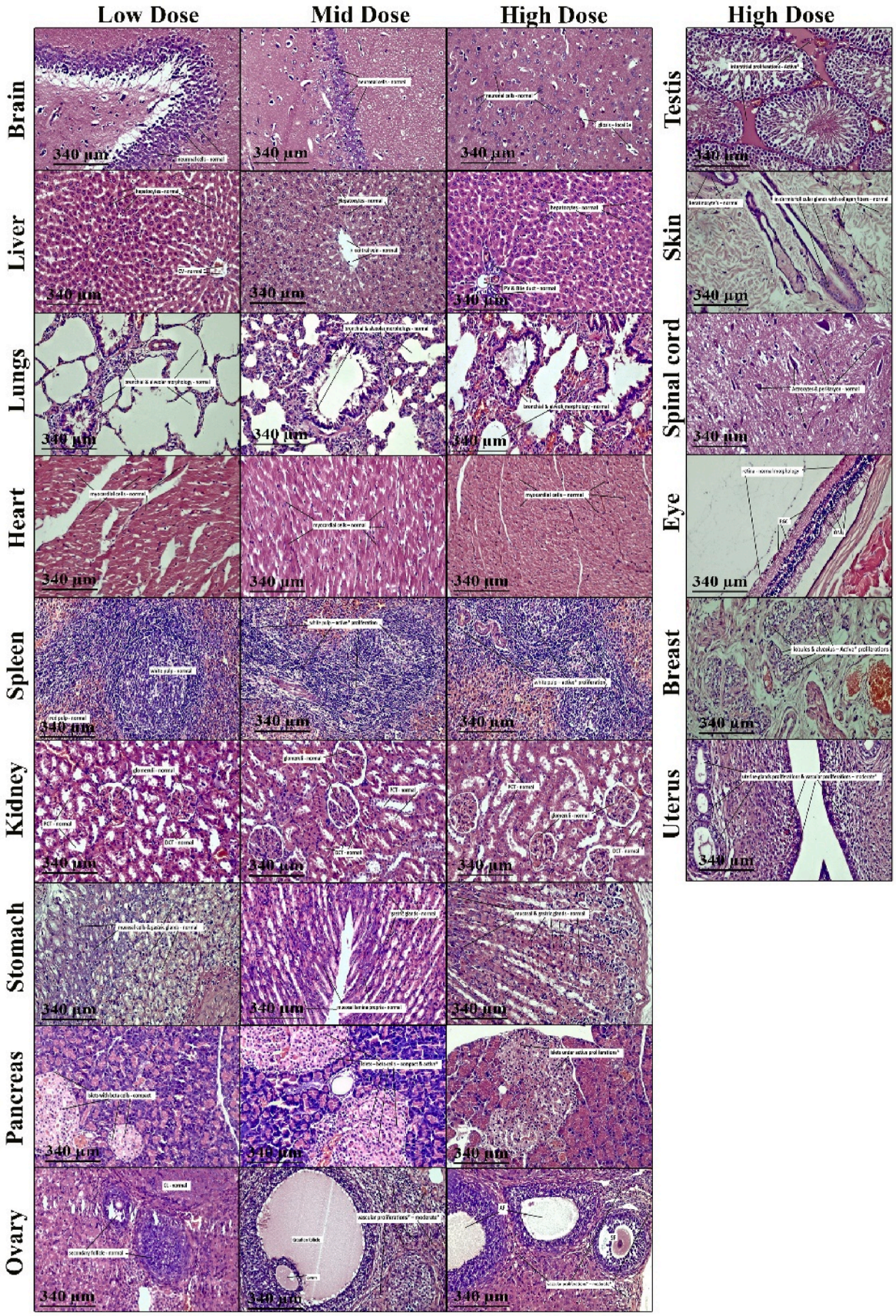

Fig. 9. Sub-acute toxicity histopathology images of FA-FeA-SWCNTs.

4.8.3. Effect of treatment on hematological parameters

Hematological parameter assessment is a reliable method for diagnosing disease. Hematological factors in breast cancer may predict the severity and subsequent course of treatment. The disease control group had significantly lower levels of hemoglobin, 7.85 ± 0.33 g/dL vs. 14.60 ± 0.30 g/dL, $p < 0.001$, along with a significant reduction in the RBC count and PCV suggesting anemic-like condition. High-dose treatment (3 mg/kg) significantly restored hemoglobin levels to 12.00 ± 0.29 g/dL, $p < 0.01$, and that of RBC count to 6.23 ± 0.25 million/μL, $p < 0.01$. At the same time, platelet counts were also improved at statistically significant levels, $p < 0.01$, shown in Fig. 10 and Table 3. These findings suggest that the treatment augment's hematopoietic function and alleviates hematological disorders, probably through enhanced erythropoiesis and decreased oxidative stress.

4.8.4. Biochemical parameter estimation

It is possible to identify if the liver has been damaged, inflamed, or functioning normally with a number of specialized blood tests. The carcinogen DMBA can cause significant oxidative damage to several body organs, including the liver, kidney and breast. The disease control group had markedly elevated levels of urea (34.50 ± 1.16 mg/dL), BUN (35.43 ± 1.42 mg/dL), and serum creatinine (1.20 ± 0.06 mg/dL). Uric acid (0.79 ± 0.02 mg/dL) compared to the normal control group, which was urea: 21.93 ± 1.77 mg/dL, BUN: 25.03 ± 1.66 mg/dL, serum creatinine: 0.60 ± 0.06 mg/dL, uric acid: 0.48 ± 0.05 mg/dL; $p <$ 0 0.001). There was a significant increase in liver enzymes SGOT (174 0.90 ± 3 0.66 U/L), SGPT (161.70 ± 3.21 U/L), ALP (113.40 ± 2.72 IU/L) and GGT (7.73 ± 0 0.18 U/L) with profound disturbance in electrolyte levels sodium (178.67 ± 1.15 mmol/L), potassium (2.33 ± 0.25 mmol/L), and chloride (120.40 ± 3.09 mmol/L). High-dose treatment at the rate of injection of 3 mg/kg resulted in the complete normalization of renal, liver and electrolyte markers (21.63 ± 1.69 mg/dL), BUN (23.30 ± 1.76 mg/dL), serum creatinine (0.60 ± 0.06 mg/dL), uric acid (0.65 ± 0.04 mg/dL), liver enzymes and sodium (122.00 ± 2.00 mmol/L), potassium (4.13 ± 0.20 mmol/L), and chloride (102.90 ± 1.68 mmol/L), shown in Figs. 11 and 12 and Table 3.

The control group for the disease showed evidence of renal and hepatic dysfunction by the raised levels of urea, BUN, serum creatinine, liver enzymes and altered electrolytes, indicating organ impairment and metabolic disruption. These parameters were significantly improved with the high-dose treatment (3 mg/kg), which normalized the markers of kidney and liver functions and corrected the electrolyte imbalances.

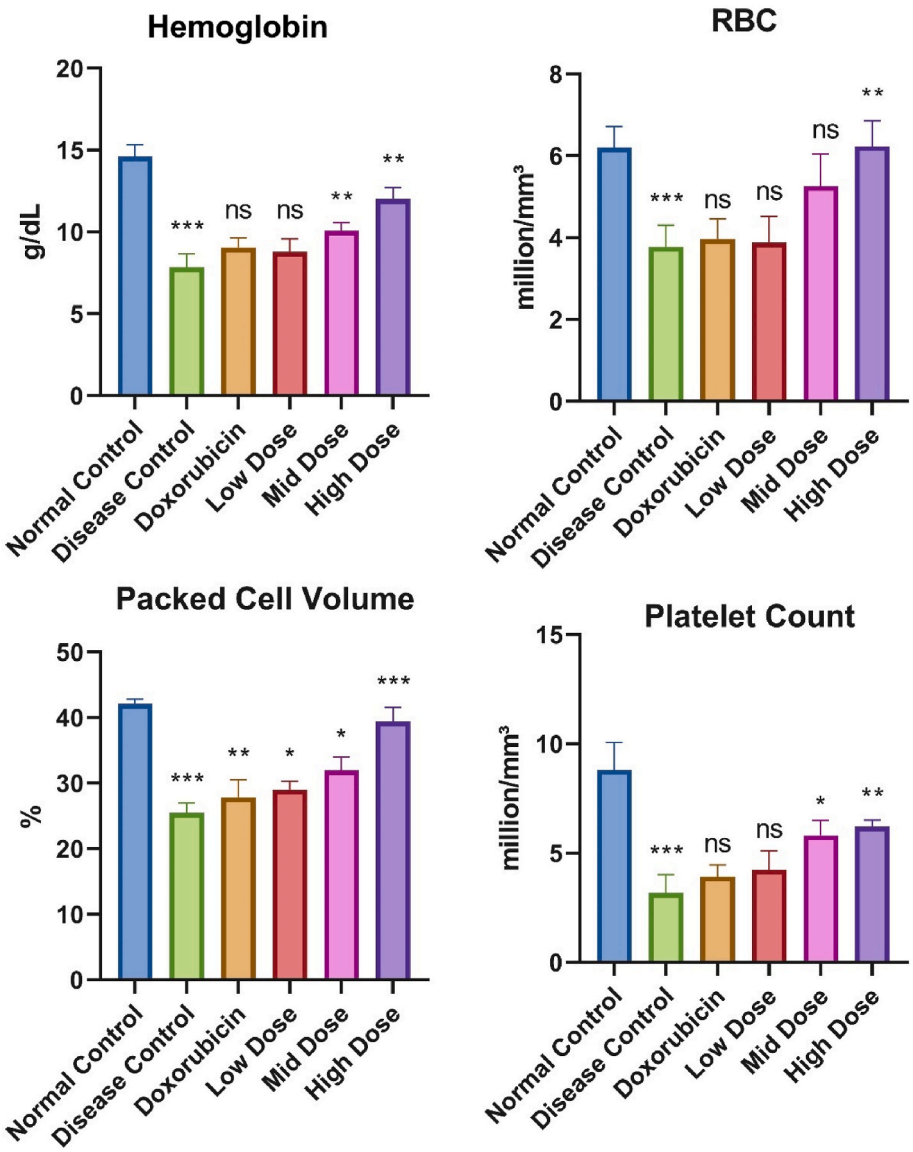

Fig. 10. Hematological evaluation of FA-FeA-SWCNTs in DMBA induced rats.

Table 3
In vivo pharmacological parameters of FA-FeA-SWCNTs in DMBA induced rats.

Parameter	Normal Control	Disease Control	Standard	Low dose (0.7 mg/kg)	Mid dose (1.5 mg/kg)	High dose (3 mg/kg)
Hematological Parameters						
Hemoglobin (g/dL)	14.60 ± 0.30	7.85 ± 0.33***	9.05 ± 0.24ns	8.78 ± 0.32ns	10.10 ± 0.19**	12.00 ± 0.29**
RBC (million/μL)	6.20 ± 0.21	3.78 ± 0.21***	3.97 ± 0.20ns	3.88 ± 0.26ns	5.27 ± 0.32ns	6.23 ± 0.25**
PCV (%)	42.08 ± 0.29	25.48 ± 0.61***	34.50 ± 0.72**	29.02 ± 0.50*	31.99 ± 0.82*	39.45 ± 0.87***
Platelet Count (lakhs/μL)	8.82 ± 0.51	3.17 ± 0.34***	3.92 ± 0.22ns	4.23 ± 0.35ns	5.82 ± 0.28*	6.22 ± 0.12**
Biochemical Evaluation						
Total Protein (g/dL)	8.32 ± 0.32	4.43 ± 0.47***	7.45 ± 0.25**	5.83 ± 0.42ns	6.28 ± 0.39*	7.17 ± 0.37**
Albumin (g/dL)	5.70 ± 0.28	2.55 ± 0.29***	5.63 ± 0.24***	3.93 ± 0.31*	4.08 ± 0.22*	4.98 ± 0.25**
Globulin (g/dL)	2.58 ± 0.19	5.85 ± 0.34***	2.83 ± 0.34***	5.50 ± 0.30ns	4.47 ± 0.19*	3.55 ± 0.28**
SGOT (U/L)	112.60 ± 2.26	174.90 ± 3.66***	132.00 ± 2.84**	157.40 ± 2.77ns	146.30 ± 3.48*	126.20 ± 2.94***
SGPT (U/L)	73.18 ± 3.24	161.70 ± 3.21***	81.95 ± 3.22***	142.10 ± 3.54ns	124.60 ± 2.98**	84.03 ± 3.49***
ALP (IU/L)	244.00 ± 5.62	113.40 ± 2.72***	233.30 ± 3.66***	174.80 ± 3.58**	191.60 ± 3.13**	224.10 ± 4.44***
Total Bilirubin (mg/dL)	0.38 ± 0.02	0.65 ± 0.02***	0.35 ± 0.03***	0.47 ± 0.02*	0.35 ± 0.02**	0.39 ± 0.02***
GGT (U/L)	4.80 ± 0.33	7.73 ± 0.18**	3.93 ± 0.27***	6.52 ± 0.23*	5.67 ± 0.33**	4.72 ± 0.30***
Uric Acid (mg/dL)	0.48 ± 0.05	0.79 ± 0.02***	0.60 ± 0.04**	0.81 ± 0.02ns	0.76 ± 0.05ns	0.65 ± 0.04*
Urea (mg/dL)	21.93 ± 1.77	34.50 ± 1.16***	22.80 ± 1.33**	30.53 ± 1.07ns	26.50 ± 1.17*	21.63 ± 1.69**
BUN (mg/dL)	25.03 ± 1.66	35.43 ± 1.42**	25.90 ± 1.14**	28.40 ± 0.98ns	27.20 ± 1.63*	23.30 ± 1.76**
Serum Creatinine (mg/dL)	0.60 ± 0.06	1.20 ± 0.06***	0.60 ± 0.06***	0.80 ± 0.06*	0.80 ± 0.06*	0.60 ± 0.06***
Sodium (mmol/L)	126.67 ± 3.06	178.67 ± 1.15***	142.00 ± 2.00**	165.00 ± 2.00ns	145.00 ± 2.00ns	122.00 ± 2.00*
Potassium (mmol/L)	5.30 ± 0.10	2.33 ± 0.25***	4.20 ± 0.20**	2.77 ± 0.20ns	3.53 ± 0.18*	4.13 ± 0.20**
Chloride (mmol/L)	101.80 ± 2.83	120.40 ± 3.09**	105.10 ± 1.75*	110.80 ± 2.78ns	108.50 ± 2.97ns	102.90 ± 1.68*
Antioxidant parameter Evaluation						
SOD (u/mg/tissue)	7.338 ± 0.061	2.885 ± 0.068***	3.415 ± 0.121ns	3.918 ± 0.034**	5.357 ± 0.153***	6.617 ± 0.162***
Catalase (u/mg/tissue)	4.145 ± 0.112	1.843 ± 0.059***	2.375 ± 0.136*	2.321 ± 0.163ns	2.539 ± 0.153ns	3.175 ± 0.113***
Glutathione (nm/100 mg)	4.410 ± 0.115	1.733 ± 0.033***	3.25 ± 0.119*	3.217 ± 0.058ns	3.9 ± 0.098ns	4.292 ± 0.078***

Values are expressed as Mean ± SEM where n = 3; One way ANOVA followed by a comparison between disease vs treatment groups using Dunnett's *t*-test, where a = $p < 0.05$, b = $p < 0.01$, c < 0.001 and d = $p < 0.0001$.

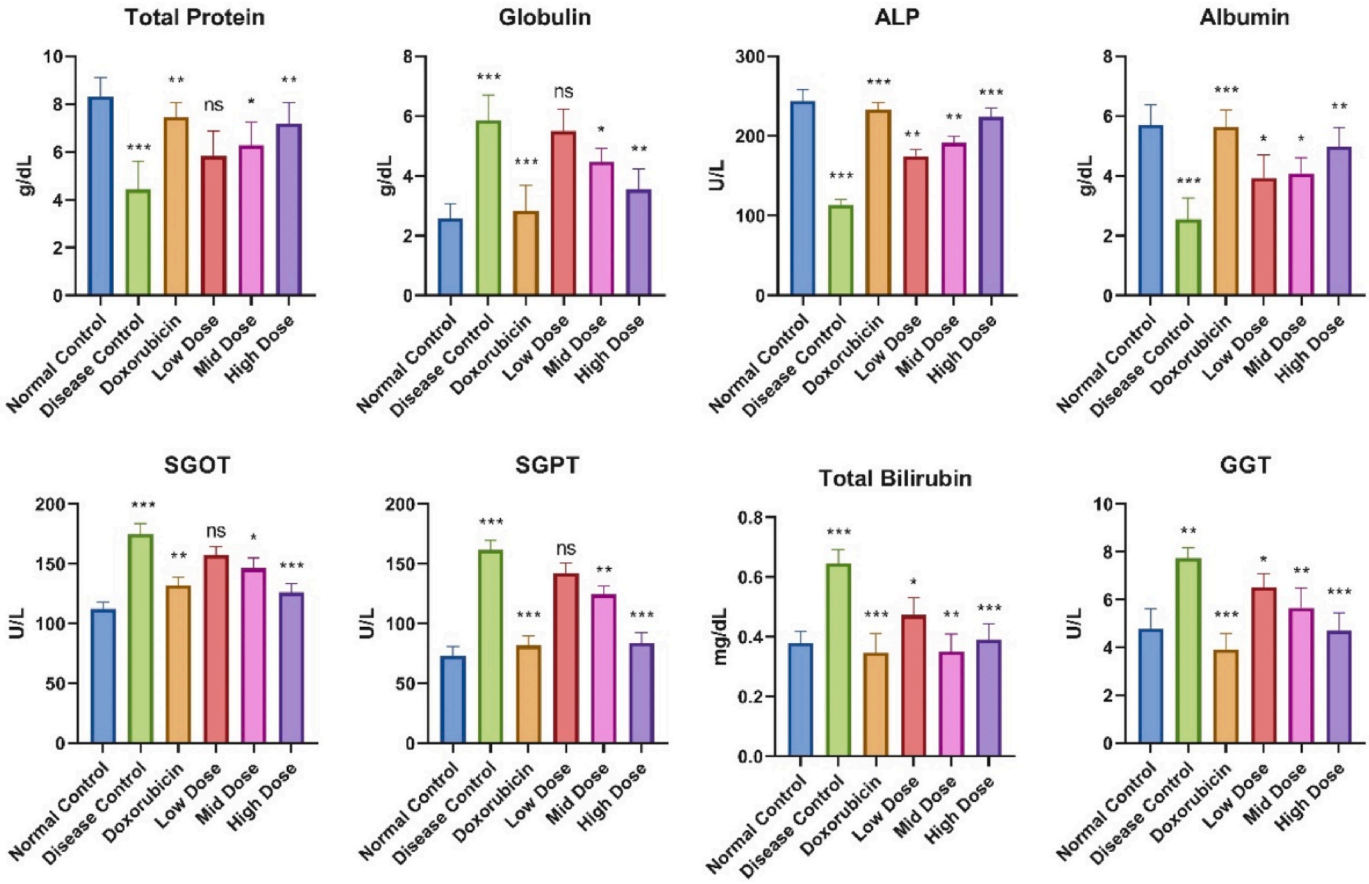

Fig. 11. Biochemical evaluation of FA-FeA-SWCNTs in DMBA induced rats liver.

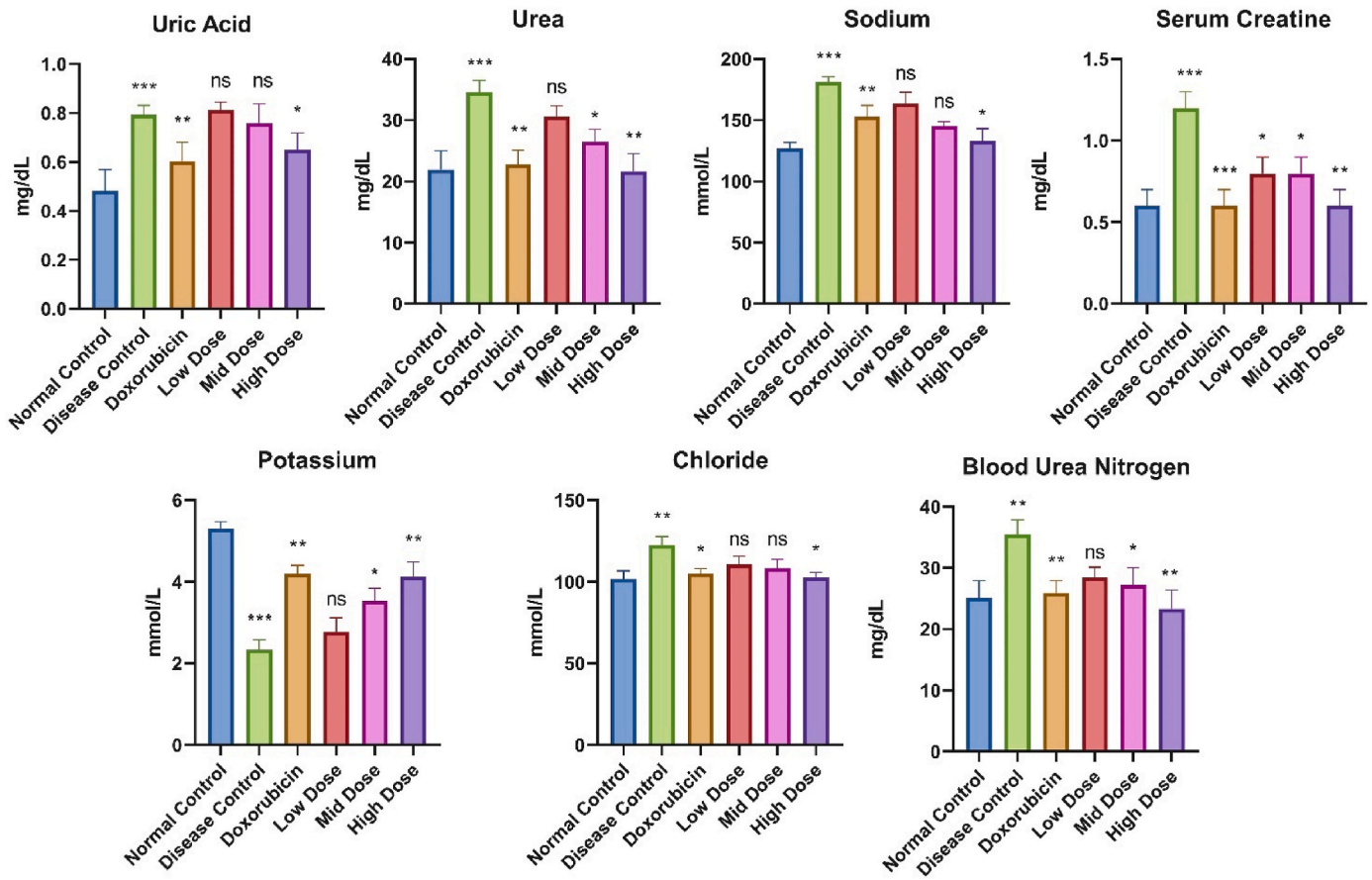

Fig. 12. Biochemical evaluation of FA-FeA-SWCNTs in DMBA induced rats lidney.

The sodium, potassium and chloride levels returned to normal values; hence, the overall metabolic balance was restored. Such findings indicate that high-dose treatment is nephroprotective and hepatoprotective, probably mediated through antioxidant and anti-inflammatory pathways that facilitate recovery of renal and hepatic functions and electrolyte homeostasis restoration.

4.8.5. Evaluation of antioxidant parameters

The disease control group exhibited significantly lower activities of the key antioxidant enzymes SOD, catalase, and glutathione compared to the normal control group. The corresponding values for the disease control group are SOD (2.885 ± 0.068 U/mg tissue), catalase (1.843 ± 0.059 U/mg tissue), and glutathione (1.733 ± 0.033 nm/100 mg) versus those of the normal control group which are SOD (7.338 ± 0.061 U/mg tissue), catalase (4.145 ± 0.112 U/mg tissue) and glutathione (4.410 ± 0.115 nm/100 mg; $p < 0.001$). Antioxidant enzyme activities were significantly increased in standard, low-dose (0.7 mg/kg), mid-dose (1.5 mg/kg) and high-dose (3 mg/kg) treatments compared to the disease control group., The high-dose treatment provided the maximum effect by bringing SOD, catalase and glutathione levels near-baseline

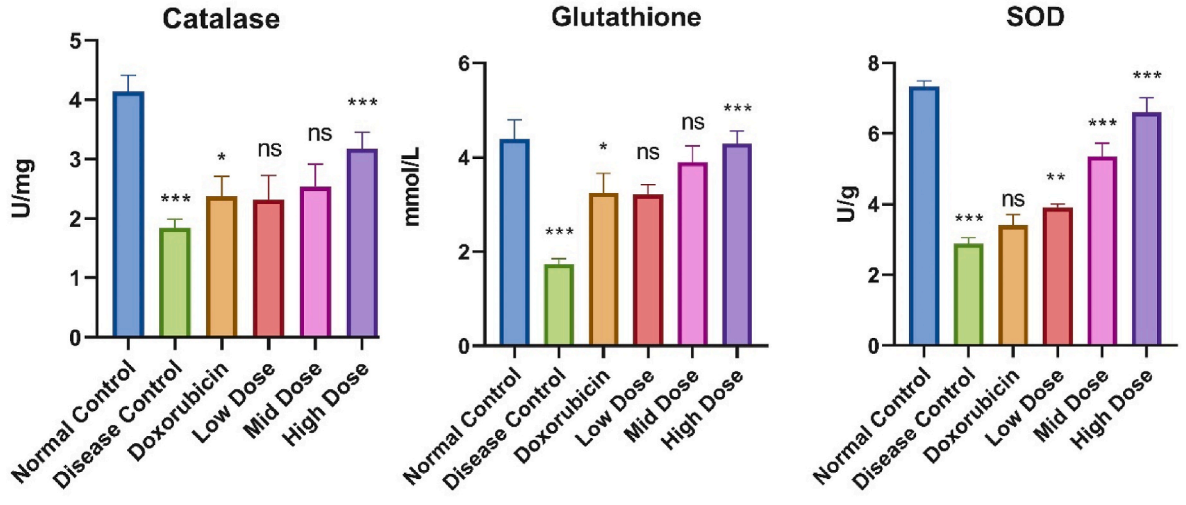

Fig. 13. Antioxidant evaluation of FA-FeA-SWCNTs in DMBA induced rats.

values; they were restored to SOD (6 0.617 ± 0.162 U/mg tissue), catalase (3 0.175 ± 0.113 U/mg tissue) and glutathione (4 0.292 ± 0 0.078 nm/100 mg), shown in Fig. 13 and Table 3.

The disease control group showed a marked decrease in antioxidant enzyme activity, which indicates oxidative stress, one of the several factors underlying the disease process. The high-dose treatment (3 mg/kg) significantly increased the activities of SOD, catalase, and glutathione, which suggests strong antioxidant effects. Restoration of these enzymes would imply decreased oxidative damage and improved cellular defense mechanisms. Perhaps the high-dose treatment protects against oxidative stress, contributing to tissue integrity and therapeutic efficacy.

4.8.6. Histopathological examination

The mammary tissue section from the control animal in the present histopathological analysis displays normal mammary tissue architecture. The breast tumor section is shown in the diseased group. This section exhibits a crisscrossed distribution of fibroblast and fibrocyte cells, which are totally displacing the mammary gland's normal adipose tissue. Since most fibrocytes are immature and have minimal vascularity, they may indicate soft fibroma. In the treatment group, the mammary gland and fibrous tissue initially showed tumorous development when induced. Breast tissue treated with FA-FeA-SWCNTs exhibited hyperkeratinisation, epithelization, scarring and tissue healing, with no signs of cancer observed.

4.8.7. Histopathological study results

Significant therapeutic responses were seen in the histopathological analysis of the breast tissue in rats treated with the FA-FeA-SWCNTs, especially in the high-dose group. Significantly, the high-dose therapy produced keratinocyte proliferation that effectively promoted epithelialization and the repair of the extracellular matrix (ECM), defined by thick dermis collagen layers. This suggests a strong healing reaction made possible by the formulation. On the other hand, the disease control group showed signs of interstitial fibrosis, ductular hyperplasia, and blood vessel congestion, which are all detrimental outcomes. Keratinocyte and ECM proliferation aided in tissue healing at both the low and mid doses of the test medication, which also showed some beneficial effects. In brief, the results prove that the FA-FeA-SWCNTs formulation can be a therapeutic candidate in breast cancer treatment since it efficiently targets malignant tissue with excellent results and, at the same time, proves to enhance healing responses in breast tissue, as shown in Fig. 14.

5. Discussion

The work emphasizes the therapeutic potential of ferulic acid and its combination with SWCNTs in the treatment of breast cancer, exposing a holistic strategy to addressing tumor growth and metastasis. The promise of FeA as an anti-cancer treatment was confirmed by molecular docking experiments, which demonstrated its versatile binding activity with targets such as Abl Kinase, VEGF receptor, and progesterone receptor, while molecular dynamics simulations confirmed its strong and stable binding to MAPK proteins. FeA demonstrated favorable pharmacokinetic characteristics, according to ADMET study, even though structural modifications are required to increase bioavailability across biological barriers. The FA-FeA-SWCNTs formulation's strong encapsulation efficiency (75.43 %) and continuous drug release ensured long-lasting therapeutic release. Strong anti-cancer effects were shown in vitro studies, which also showed that it reduced MCF-7 cell viability on par with doxorubicin and prevented neovascularization by inhibiting the growth of new blood vessels.

The potential of FeA to reverse the epithelial-mesenchymal transition (EMT) sets it apart from existing nanotherapeutics such liposomal doxorubicin and albumin-bound paclitaxel, which primarily target tumor cytotoxicity without addressing metastatic pathways. FeA-induced EMT reversal is important in aggressive forms of breast cancer because it particularly targets the major pathways behind metastasis. Like PLGA-based nanoparticles, FA-FeA-SWCNTs exhibit a prolonged drug release profile, a dual mode of action of tumor suppression and metastasis inhibition, and reflect FeA's antioxidant and anti-angiogenic properties. With only mild hepatic stress observed at high therapeutic doses, the FA-FeA-SWCNTs formulation was found to have a good safety profile in rodents when compared to other nanotherapies that are prone to toxicity issues like cardiotoxicity or immunological responses.

By observing the dramatic decrease in tumor diameters of treated animals and the improvement in their hematological and biochemical parameters, the *in vivo* investigations further confirmed the dose-dependent anti-tumor actions of FA-FeA-SWCNTs. Breast tissue histopathology revealed epithelialization and tissue healing, which further validated the formulation as a treatment strategy for breast cancer. Comparing SWCNT encapsulation to alternative FeA-based delivery technologies such as electrospun nanofibers or folate-targeted PLGA nanoparticles, it is found to enhance the bioavailability and therapeutic effectiveness of FeA while maintaining safety.

Ferulic Acid's poor bioavailability, which comes from its limited permeability across biological barriers and low water solubility, is a

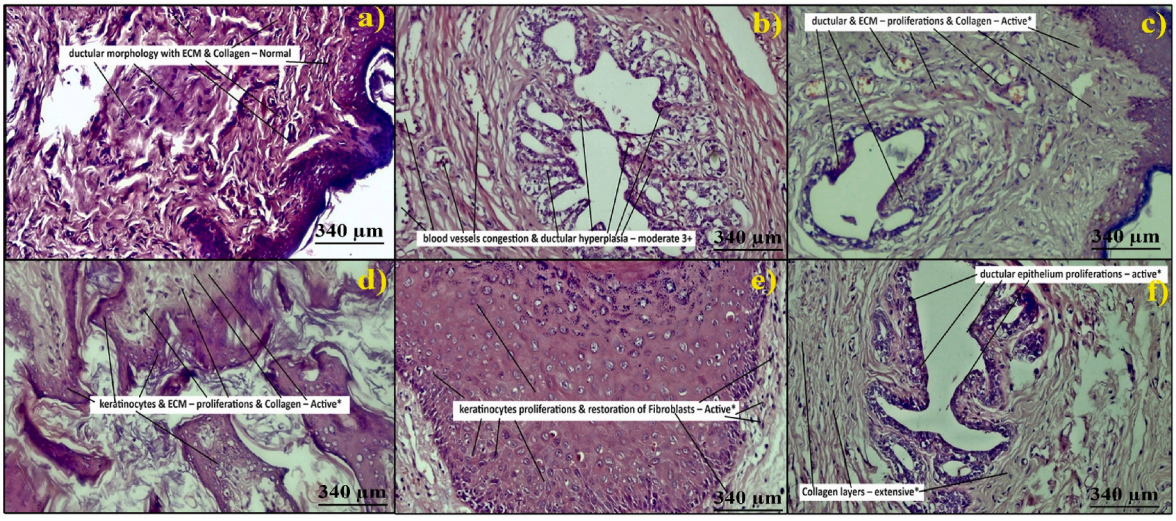

Fig. 14. Histopathology images of FA-FeA-SWCNTs in DMBA induced rats: a) Normal control; b) Disease control; c) Standard drug; d) Low dose test drug; e) Mid dose test drug; f) High dose test drug.

major disadvantage. The human body finds it difficult to absorb as a result, necessitating repeated dosage. Encapsulation within SWCNTs improves drug delivery and stability, but more structural changes are needed to optimize efficacy. Adjusting the dose at high concentrations to decrease hepatic stress is still challenging. To enhance outcomes, future research should explore combination therapy with radiation or immune checkpoint inhibitors and leverage the optical properties of SWCNTs for imaging-guided theranostic applications. FA-FeA-SWCNTs is a significant advancement in naturally derived nanotherapeutics, providing a dual mechanism of tumor suppression and metastasis inhibition together with a favorable safety profile compared to existing therapies.

6. Conclusion

Undoubtedly, FA-FeA-SWCNTs formulation proves to be a new dimension in breast cancer treatment. The combination of folic acid targeting, Ferulic Acid therapeutic properties and efficient delivery mechanism of single-walled carbon nanotubes show this formulation as a potential new strategy for fighting against cancer in an effective way. The unique anti-cancer activity shown in *in-vitro* and animal studies reflect its ability to inhibit tumor growth and lessen the formation of new blood vessels which nourish tumors. Moreover, the formulation has favorable safety profiles, making it well-suited for patient acceptance, which is important for any cancer treatment. As researchers continue to explore the potential for further development in clinical settings, there is hope to find better treatment options for breast cancer patients. Overall, the FA-FeA-SWCNTs formulation shows promise in providing less harmful and more effective therapies, ultimately contributing to a better quality of life for breast cancer patients.

CRediT authorship contribution statement

Sandra Ross Olakkengil Shajan: Writing – original draft. **Shivaraj Kumar Walikar:** Data curation. **Nandini Markuli Sadashivappa:** Data curation. **Devaraj Hanumanthappa:** Resources. **Basavana Gowda Hosur Dinesh:** Validation, Resources. **Bandral Sunil Kumar:** Validation, Resources. **Srinivas Ganjipete:** Software, Resources. **Selvaraj Kunjiappan:** Supervision, Methodology. **Sankaranarayanan Murugesan:** Software, Resources. **Panneerselvam Theivendren:** Visualization, Validation. **Kumarappan Chidambaram:** Validation, Resources. **Damodar Nayak Ammunje:** Validation, Supervision, Investigation. **Parasuraman Pavadai:** Writing – review & editing, Supervision, Conceptualization.

Ethics approval and consent to participate

All procedures involving experimental animals were performed after obtaining prior approval from the Institutional Animal Ethical Committee (Approved number: XXVIII/MSRFPH/COL/PG-06/November 15, 2023).

Consent for publication

Not applicable.

Funding

No external funding was received.

Declaration of competing interest

The authors declare that they have no known competing financial interests or personal relationships that could have appeared to influence the work reported in this paper.

Acknowledgments

The authors would like to thank M.S. Ramaiah University of Applied Sciences, Bengaluru, India for supporting this project by providing the necessary facilities. -The authors extend their appreciation to the Deanship of Scientific Research and Graduate Studies at King Khalid University for funding this work through a Large Group Research Project under grant number RGP.2/189/46.

Appendix A. Supplementary data

Supplementary data to this article can be found online at https://doi.org/10.1016/j.jddst.2025.107111.

Data availability

Data will be made available on request.

References

[1] S.G. Morounke, J.B. Ayorinde, A.O. Benedict, F.F. Adedayo, F.O. Adewale, I. Oluwadamilare, S.S. Sokunle, A. Benjamin, Epidemiology and incidence of common cancers in Nigeria, Population (Paris) 84 (82,231,000) (2017) 166–629.
[2] K. Yoshida, Y. Miki, Role of BRCA1 and BRCA2 as regulators of DNA repair, transcription, and cell cycle in response to DNA damage, Cancer Sci. 95 (11) (2004) 866–871.
[3] I. Humans, I.W. Group, Tobacco smoke and involuntary smoking, IARC Monogr. Eval. Carcinog. Risks Hum. 83 (2004) 1–1438.
[4] T.-H. Sin, J. Huang, L. Nie, F. Mao, S. Shen, Y. Li, Q. Sun, J. Lu, X. Zhang, Y. Zhou, Successful treatment of enormous locally advanced breast cancer through neoadjuvant chemotherapy and surgical intervention: a case report, Gland Surg. 13 (6) (2024) 1126.
[5] M.I. Nounou, F. ElAmrawy, N. Ahmed, K. Abdelraouf, S. Goda, H. Syed-Sha-Qhattal, Breast cancer: conventional diagnosis and treatment modalities and recent patents and technologies, Breast Cancer Basic Clin. Res. 9 (2015). BCBCR. S29420.
[6] T. Khan, M. Ali, A. Khan, P. Nisar, S.A. Jan, S. Afridi, Z.K. Shinwari, Anticancer plants: a review of the active phytochemicals, applications in animal models, and regulatory aspects, Biomolecules 10 (1) (2019) 47.
[7] S. Nakonieczna, A. Grabarska, W. Kukula-Koch, The potential anticancer activity of phytoconstituents against gastric cancer—A review on in vitro, in vivo, and clinical studies, Int. J. Mol. Sci. 21 (21) (2020) 8307.
[8] S. Shukla, A. Mehta, Anticancer potential of medicinal plants and their phytochemicals: a review, Braz. J. Bot. 38 (2015) 199–210.
[9] S. Prakash, N. Elavarasan, K. Subashini, S. Kanaga, R. Dhandapani, M. Sivanandam, P. Kumaradhas, C. Thirunavukkarasu, V. Sujatha, Isolation of hesperetin-A flavonoid from Cordia sebestena flower extract through antioxidant assay guided method and its antibacterial, anticancer effect on cervical cancer via in vitro and in silico molecular docking studies, J. Mol. Struct. 1207 (2020) 127751.
[10] D. Li, Y.-x. Rui, S.-d. Guo, F. Luan, R. Liu, N. Zeng, Ferulic acid: a review of its pharmacology, pharmacokinetics and derivatives, Life Sci. 284 (2021) 119921.
[11] N. Kumar, V. Pruthi, Potential applications of ferulic acid from natural sources, Biotechnol. Rep. 4 (2014) 86–93.
[12] P. Mattila, J. Hellström, Phenolic acids in potatoes, vegetables, and some of their products, J. Food Compos. Anal. 20 (3–4) (2007) 152–160.
[13] P. Mattila, J. Hellström, R. Törrönen, Phenolic acids in berries, fruits, and beverages, J. Agric. Food Chem. 54 (19) (2006) 7193–7199.
[14] P. Mattila, J.-m. Pihlava, J. Hellström, Contents of phenolic acids, alkyl-and alkenylresorcinols, and avenanthramides in commercial grain products, J. Agric. Food Chem. 53 (21) (2005) 8290–8295.
[15] N. Kour, G. Bhagat, S. Singh, S.S. Bhatti, S. Arora, B. Singh, A. Bhatia, Polyphenols mediated attenuation of diabetes associated cardiovascular complications: a comprehensive review, J. Diabetes Metab. Disord. 23 (1) (2024) 73–99.
[16] M. Srinivasan, A.R. Sudheer, V.P. Menon, Ferulic acid: therapeutic potential through its antioxidant property, J. Clin. Biochem. Nutr. 40 (2) (2007) 92–100.
[17] D.N. Dikmetas, H. Yenipazar, A.C. Karaca, Recent advances in encapsulation of resveratrol for enhanced delivery, Food Chem. (2024) 140475.
[18] M. ElKhazendar, J. Chalak, W. El-Huneidi, A. Vinod, W.M. Abdel-Rahman, E. Abu-Gharbieh, Antiproliferative and proapoptotic activities of ferulic acid in breast and liver cancer cell lines, Trop. J. Pharmaceut. Res. 18 (12) (2019) 2571–2576.
[19] J.W. Locasale, Serine, glycine and one-carbon units: cancer metabolism in full circle, Nat. Rev. Cancer 13 (8) (2013) 572–583.
[20] L.S. Boogerd, M.C. Boonstra, A.-J. Beck, A. Charehbili, C.E. Hoogstins, H.A. Prevoo, S. Singhal, P.S. Low, C.J. van de Velde, A.L. Vahrmeijer, Concordance of folate receptor-α expression between biopsy, primary tumor and metastasis in breast cancer and lung cancer patients, Oncotarget 7 (14) (2016) 17442.
[21] L.C. Hartmann, G.L. Keeney, W.L. Lingle, T.J. Christianson, B. Varghese, D. Hillman, A.L. Oberg, P.S. Low, Folate receptor overexpression is associated with poor outcome in breast cancer, Int. J. Cancer 121 (5) (2007) 938–942.
[22] S.R.O. Shajan, N.M. Sadashivappa, D. Hanumanthappa, S.K. Walikar, B.G. H. Dinesh, B.S. Kumar, S. Kunjiappan, P. Theivendren, S.K.K. Alagarsamy,

K. Chidamabaram, Exploring the potential application of single-walled carbon nanotubes in medical treatment and therapy, Talanta Open (2024) 100392.
[23] S. Pattnaik, Y. Surendra, J.V. Rao, K. Swain, Carbon family nanomaterials for drug delivery applications. Nanoengineered Biomaterials for Advanced Drug Delivery, Elsevier, 2020, pp. 421–445.
[24] J.M. González-Domínguez, M.Á. Álvarez-Sánchez, C. Hadad, A.M. Benito, W. K. Maser, Carbon nanostructures and polysaccharides for biomedical materials, in: T. Da Ros, N. Martín, J.-F. Nierengarten (Eds.), Carbon Nanostructures for Biomedical Applications, The Royal Society of Chemistry, 2021.
[25] H.-K. Min, C.-S. Kim, J. Han, J.-O. Park, E. Choi, Folate receptor-targeted liposomal nanocomplex for effective synergistic photothermal-chemotherapy of breast cancer in vivo, Colloids Surf., B Biointerfaces 173 (2019) 539–548.
[26] S. Kunjiappan, M. Sankaranarayanan, B.K. Kumar, P. Pavadai, E. Babkiewicz, P. Maszczyk, E. Glodkowska-Mrowka, S. Arunachalam, S.R.K. Pandian, V. Ravishankar, Capsaicin-loaded solid lipid nanoparticles: design, biodistribution, in silico modeling and in vitro cytotoxicity evaluation, Nanotechnology (Bristol) 32 (9) (2020).
[27] B. Kumar, P. Parasuraman, T.P.K. Murthy, M. Murahari, V. Chandramohan, In silico screening of therapeutic potentials from Strychnos nux-vomica against the dimeric main protease (mpro) structure of SARS-CoV-2, J. Biomol. Struct. Dyn. 40 (17) (2022) 7796–7814.
[28] A.K. Kalimuthu, P. Parasuraman, P. Sivakumar, S. Murugesan, S. Arunachalam, S. R.K. Pandian, V. Ravishankar, D.N. Ammunje, M. Sampath, T. Panneerselvam, In silico, in vitro screening of antioxidant and anticancer potentials of bioactive secondary metabolites from an endophytic fungus (curvularia sp.) from Phyllanthus niruri L, Environ. Sci. Pollut. Control Ser. 29 (32) (2022) 48908–48925.
[29] S. Vellur, P. Pavadai, E. Babkiewicz, S. Ram Kumar Pandian, P. Maszczyk, S. Kunjiappan, An in silico molecular modelling-based prediction of potential Keap1 inhibitors from Hemidesmus indicus (L.) R. Br. against oxidative-stress-induced diseases, Molecules (Basel) 28 (11) (2023) 4541.
[30] J. Chandrasekaran, S. Elumalai, V. Murugesan, S. Kunjiappan, P. Pavadai, P. Theivendren, Computational design of PD-L1 small molecule inhibitors for cancer therapy, Mol. Divers. 27 (4) (2023) 1633–1644.
[31] S. Kunjiappan, S. Govindaraj, P. Parasuraman, M. Sankaranarayanan, S. Arunachalam, P. Palanisamy, U.P. Mohan, E. Babkiewicz, P. Maszczyk, S. Vellaisamy, Design, in silico modelling and functionality theory of folate-receptor-targeted myricetin-loaded bovine serum albumin nanoparticle formulation for cancer treatment, Nanotechnology (Bristol) 31 (15) (2020) 155102.
[32] S. Kunjiappan, T. Panneerselvam, P. Pavadai, V. Balakrishnan, S.R.K. Pandian, P. Palanisamy, M. Sankaranarayanan, S.J. Kabilan, G.A. Sundaram, W.-L. Tseng, Fabrication of folic acid-conjugated pyrimidine-2 (5H)-thione-encapsulated curdlan gum-PEGamine nanoparticles for folate receptor targeting breast cancer cells, Int. J. Biol. Macromol. 277 (2024) 134406.
[33] R.R. Rajeshkumar, P. Pavadai, T. Panneerselvam, V. Deepak, S.R.K. Pandian, S. J. Kabilan, S. Vellaichamy, A. Jeyaraman, A.S.K. Kumar, K. Sundar, Glucose-conjugated glutenin nanoparticles for selective targeting and delivery of camptothecin into breast cancer cells, N. Schmied. Arch. Pharmacol. 396 (10) (2023) 2571–2586.
[34] R.R. Rajeshkumar, T. Panneerselvam, P. Pavadai, S.R.K. Pandian, A.S.K. Kumar, M. Sankaranarayan, S.J. Kabilan, S. Kunjiappan, Folate receptor-targeted Camptothecin-loaded PLGA-glutenin nanoparticles for effective breast cancer treatment, J. Polym. Environ. 32 (12) (2024) 6440–6460.
[35] S. Baskararaj, T. Panneerselvam, S. Govindaraj, S. Arunachalam, P. Parasuraman, S.R.K. Pandian, M. Sankaranarayanan, U.P. Mohan, P. Palanisamy, V. Ravishankar, Formulation and characterization of folate receptor-targeted PEGylated liposome encapsulating bioactive compounds from Kappaphycus alvarezii for cancer therapy, 3 Biotech 10 (3) (2020) 136.
[36] S. Kunjiappan, T. Panneerselvam, S. Govindaraj, P. Parasuraman, S. Baskararaj, M. Sankaranarayanan, S. Arunachalam, E. Babkiewicz, A. Jeyakumar, M. Lakshmanan, Design, in silico modelling, and functionality theory of novel folate receptor targeted rutin encapsulated folic acid conjugated keratin nanoparticles for effective cancer treatment, Anti-Cancer Agents Med. Chem.Anti-Cancer Agents 19 (16) (2019) 1966–1982.
[37] R.R. Rajeshkumar, P. Pavadai, T. Panneerselvam, S.R.K. Pandian, A.S.K. Kumar, P. Maszczyk, E. Babkiewicz, S.J. Kabilan, S. Kunjiappan, Enhanced delivery of retinoic acid to breast cancer cells by folate receptor-targeted folic acid-conjugated glutenin nanoparticles for promising treatment of breast cancer, J. Polym. Environ. 32 (5) (2024) 2120–2139.
[38] G.A. Mariya, M. Ramar, L.J.K. Henry, S. Natesan, R. Kandasamy, Fabrication of chitosan-based redox-responsive polymeric nanoparticles: in-vitro and in-vivo evaluation for treating airway inflammation in asthma, J. Drug Deliv. Sci. Technol. 84 (2023) 104473.
[39] U. Yapa Bandara, P. Soysa, C. Witharana, Induction of apoptosis and antiproliferative activity of MCF-7 human breast cancer cells with sonicated aqueous peel extract of Punica granatum L.(Nimali sp.), Asian Pac. J. Cancer Prev. APJCP 25 (11) (2024) 3967–3976.
[40] A. Riyasdeen, R. Senthilkumar, V.S. Periasamy, P. Preethy, S. Srinag, M. Zeeshan, H. Krishnamurthy, S. Arunachalam, M.A. Akbarsha, Antiproliferative and apoptosis-induction studies of a metallosurfactant in human breast cancer cell MCF-7, RSC Adv. 4 (91) (2014) 49953–49959.
[41] C. Pan, G. Zhu, Y. Zhang, X. Rao, H. Jiang, J. Pan, Light optimization for an LED-based candling system and detection combined with egg parameters for discrimination of fertility, Transact. ASABE 64 (2) (2021) 485–493.
[42] J.V. Beladiya, A.A. Mehta, Acute and 28-days subacute toxicity studies of Gαq-RGS2 signaling inhibitor, Laboratory Animal Res. 37 (2021) 1–10.
[43] M.K. Ramar, K. Chidambaram, B. Chandrasekaran, R. Kandasamy, Standardization, in-silico and in-vivo safety assessment of methanol extract of Ziziphus mauritiana lam leaves, Regul. Toxicol. Pharmacol. 131 (2022) 105144.
[44] R. Mohankumar, S.E.L. Prakash, N. Irfan, S. Mohanraj, C. Kumarappan, Evaluation of analgesic, anti-inflammatory, and antipyretic activities of Ziziphus Mauritania lam leaves in animal models, Pharmacol. Res.-Modern Chinese Med. 4 (2022) 100153.
[45] S.D. Almeida, S.H. Ramesh, G.K. Radhakrishna, G. Sireesha, S. Ramesh, B. S. Kumar, B.G. Hosur Dinesh, S. Ganjipete, S. Nagaraj, P. Theivendren, Development and evaluation of S-carboxymethyl-L-cystine-loaded solid lipid nanoparticles for Parkinson's disease in murine and zebrafish models, Sci. Rep. 15 (1) (2025) 10885.
[46] G.K. Radhakrishna, S.H. Ramesh, S.D. Almeida, G. Sireesha, S. Ramesh, P. Theivendren, A. Kumar, K. Chidamabaram, D.N. Ammunje, S. Kunjiappan, Capsaicin-entangled multi-walled carbon nanotubes against breast cancer: a theoretical and experimental approach, J. Cluster Sci. 35 (8) (2024) 2849–2869.
[47] T. Ellappan, M. Ramar, R. Manikrishnan, S.G. Melepuram, P. Balaji, V.K. Sekar, K. Chidambaram, Protective effect of Ceiba pentandra (L) Gaertn on CCl4-induced oxidative stress and liver damage in rats, Pharmacol. Res.-Modern Chinese Med. 5 (2022) 100196.
[48] M.K. Ramar, L.J.K. Henry, S. Ramachandran, K. Chidambaram, R. Kandasamy, Ziziphus mauritiana Lam attenuates inflammation via downregulating NFκB pathway in LPS-stimulated RAW 264.7 macrophages & OVA-induced airway inflammation in mice models, J. Ethnopharmacol. 295 (2022) 115445.